AMERICAN SOCIETY FOR MICROBIOLOGY | Journal of Virology®

VIRUS-CELL INTERACTIONS

TMEM45B Interacts with Sindbis Virus Nsp1 and Nsp4 and Inhibits Viral Replication

Feixiang Yan,[a,b] Wei Yang,[a] Xinlu Wang,[a,b] Guangxia Gao[a,b]

[a]CAS Key Laboratory of Infection and Immunity, Institute of Biophysics, Chinese Academy of Sciences, Beijing, China
[b]University of Chinese Academy of Sciences, Beijing, China

ABSTRACT Alphavirus infection induces the expression of type I interferons, which inhibit the viral replication by upregulating the expression of interferon-stimulated genes (ISGs). Identification and mechanistic studies of the antiviral ISGs help to better understand how the host controls viral infection and help to better understand the viral replication process. Here, we report that the ISG product TMEM45B inhibits the replication of Sindbis virus (SINV). TMEM45B is a transmembrane protein that was detected mainly in the *trans*-Golgi network, endosomes, and lysosomes but not obviously at the plasma membrane or endoplasmic reticulum. TMEM45B interacted with the viral nonstructural proteins Nsp1 and Nsp4 and inhibited the translation and promoted the degradation of SINV RNA. TMEM45B overexpression rendered the intracellular membrane-associated viral RNA sensitive to RNase treatment. In line with these results, the formation of cytopathic vacuoles (CPVs) was dramatically diminished in TMEM45B-expressing cells. TMEM45B also interacted with Nsp1 and Nsp4 of chikungunya virus (CHIKV), suggesting that it may also inhibit the replication of other alphaviruses. These findings identified TMEM45B as an antiviral factor against alphaviruses and help to better understand the process of the viral genome replication.

IMPORTANCE Alphaviruses are positive-stranded RNA viruses with more than 30 members. Infection with Old World alphaviruses, which comprise some important human pathogens such as chikungunya virus and Ross River virus, rarely results in fatal diseases but can lead to high morbidity in humans. Infection with New World alphaviruses usually causes serious encephalitis but low morbidity in humans. Alphavirus infection induces the expression of type I interferons, which subsequently upregulate hundreds of interferon-stimulated genes. Identification and characterization of host antiviral factors help to better understand how the viruses can establish effective infection. Here, we identified TMEM45B as a novel interferon-stimulated antiviral factor against Sindbis virus, a prototype alphavirus. TMEM45B interacted with viral proteins Nsp1 and Nsp4, interfered with the interaction between Nsp1 and Nsp4, and inhibited the viral replication. These findings provide insights into the detailed process of the viral replication and help to better understand the virus-host interactions.

KEYWORDS Sindbis virus, TMEM45B, virus host interaction

Alphaviruses are positive-stranded RNA viruses (1, 2). The alphavirus virion consists of a single-stranded RNA (ssRNA) genome of about 11 to 12 kb surrounded by a capsid shell and a lipid bilayer with embedded glycoproteins (3). The 5′- and 3′-terminal noncoding regions of the viral RNA flank two open reading frames (ORFs), which are separated by an internal noncoding region. The 5′ ORF encodes the nonstructural proteins Nsp1 to Nsp4, translated directly from the genomic RNA. The 3′ ORF encodes the structural proteins, which are expressed from the subgenomic RNA. The subgenomic RNA is transcribed via a subgenomic promoter from a negative-strand RNA intermediate.

Editor Susana López, Instituto de Biotecnologia/UNAM

Address correspondence to Guangxia Gao, gaogx@moon.ibp.ac.cn.

The authors declare no conflict of interest.

Received 12 June 2022
Accepted 20 July 2022
Published 8 August 2022

Alphavirus entry into the host cell is initiated by receptor binding. After receptor binding, viral particles are internalized through clathrin-mediated endocytosis (4). The clathrin coat is subsequently removed, and the virus-containing vesicles enter the early endosomal compartment. Acidification of the endosome causes exposure of the hydrophobic fusion loop of the viral E1 protein, which triggers membrane fusion (5–7). Once the nucleocapsid is released into the cytoplasm, it is disassembled, liberating the viral genomic RNA for translation (8, 9).

The 5′ ORF is translated into the nonstructural polyproteins P1234 or P123, which are assembled and transported to the membranous organelles and plasma membrane. The polyproteins bind to the membranes through the specific alpha-helical peptide and palmitoylated amino acids of Nsp1 (10–12). After the first cleavage event mediated by the Nsp2-associated protease activity, the initially formed replication complexes (RCs) contain Nsp123 and Nsp4 for synthesis of the negative-strand RNA on the genomic RNA template to form the double-stranded RNA (dsRNA) replication intermediate (13, 14). The subsequent processing of Nsp123 into Nsp1, Nsp2, and Nsp3 transforms spherule-associated RCs into the mature form that is active in genomic and subgenomic RNA synthesis (13, 15, 16).

Nsp1 can catalyze the capping reaction of newly synthesized viral genomic and subgenomic RNA (17, 18). Nsp2 has an RNA helicase activity and a protease activity for polyprotein processing and facilitates the capping of a newly synthesized viral RNA as an RNA 5′-triphosphatase (19). Nsp4 is an RNA-dependent RNA polymerase, the core subunit of viral RC (20–22). Nsp3 is a heavily phosphorylated protein (23, 24) whose macrodomain is critical for initiation of virus replication (25) and affects neurovirulence in mice (26).

Viral genome replication occurs initially at the plasma membrane in spherules, which are then endocytosed and fused with early endosomes and lysosomes to form stable, large, acidic compartments termed cytopathic vacuoles (CPV-I) (11, 27, 28). The dsRNA synthesis could modulate spherule size (29). CPV-I structures are derived from modified endosomes and lysosomes (28, 30, 31). In the late stage of infection, *trans*-Golgi network (TGN)-derived vacuoles marked with the E1/E2 glycoproteins become predominant (32, 33).

Alphavirus infection induces the expression of type I interferons (IFN). IFN protects cells from virus infection by inducing interferon-stimulated genes (ISGs) (34–36). Multiple ISGs have been reported to inhibit alphavirus replication. IFITM3 is a transmembrane protein that inhibits endosomal fusion of multiple alphaviruses (37, 38). OAS3, a member of the 2′-5′-oligoadenylate synthetase (OAS) family, inhibits the replication of chikungunya virus (CHIKV), Sindbis virus (SINV), and Semliki Forest virus (SFV) (39). OAS3 produces 2′-5′-oligoadenylates in response to dsRNA, activating RNase L to cleave the viral ssRNAs to suppress translation (40). IFIT1 selectively inhibits the translation of the viral RNA that lacks 2′-O-methylation at the 5′ end (41). However, the secondary structure elements in the 5′ untranslated regions (UTR) of Venezuelan equine encephalitis virus (VEEV) and SINV prevent IFIT1 binding to some extent (42). Variability within the 5′ secondary structure of different strains and species of alphaviruses results in a range of susceptibilities to IFIT1 (43). ZAP (PARP13) inhibits the replication of multiple alphaviruses by inhibiting the translation and promoting the degradation of the viral RNA (44). Other members of the PARP family (PARP7, PARP10, and PARP12) also inhibit alphavirus replication by repressing translation (45, 46). BST-2 inhibits the virion release of SFV and CHIKV (47). Other ISGs that have been reported to inhibit alphavirus replication include MxA (48), ISG15 (49–51), and promyelocytic leukemia zinc finger (PLZF) (52). The mechanisms of action of these ISGs are not well defined.

Here, we screened a subset of ISGs that we recently identified for their activity in inhibiting the replication of SINV and identified TMEM45B as a potent inhibitor. TMEM45B interacts with the RC components Nsp1 and Nsp4 and interferes with the interaction between Nsp1 and Nsp4 to impede the replication of the viral genome.

RESULTS

TMEM45B inhibits SINV replication. To identify novel host antiviral factors against SINV, we screened a subset of ISGs we recently reported (53). To facilitate the screening, a replication-competent SINV virus expressing a nanoluciferase reporter, SVNI-Nsp3-nLuc, was utilized. In this reporter virus, the coding sequence of nanoluciferase (nLuc) was inserted into that of Nsp3 of SVNI (Fig. 1A), a neural invasive strain of SINV (54). Viral replication is expected to result in expression of the nLuc reporter, and thus nLuc activity can serve as an indicator of the viral replication. The ISG proteins were myc tagged at the C terminus and transiently expressed in 293T cells, followed by infection of the cells with the reporter virus. nLuc activity in the infected cells was measured at 24 h postinfection and served as an indicator of the viral replication. Of the approximately 100 ISGs we screened, TMEM45B displayed significant inhibitory activity against the viral replication (Table 1). TMEM45B is a membrane protein with seven putative transmembrane domains, and the fourth to seventh transmembrane domains have been reported to confer the protein thermal aggregation properties (55). It has been reported that silencing TMEM45B inhibited cell proliferation and invasion in osteosarcoma, gastric cancer, and prostate cancer (56–58). However, the underlying mechanisms are not clear.

The antiviral activity of TMEM45B was further validated. NZAP-Zeo, which is a fusion protein comprising the N-terminal domain of the zinc finger antiviral protein (ZAP) and the Zeocin resistance gene product (Zeo) and which was previously reported to potently inhibit SINV replication (44), was used as a positive control. XAF1, an ISG that did not display any antiviral activity in the above-mentioned screening (Table 1), was used as a negative control. For comparison, TMEM45B and TMEM45C were also included. Consistent with the above-described results, TMEM45B significantly inhibited SINV replication (Fig. 1B). In contrast, TMEM45A, TMEM45C, or XAF1 did not show any antiviral activity (Fig. 1B). We noticed that the inhibition of TMEM45B against SINV was only about 10-fold in this assay, while it was 46-fold in the screening (Table 1). A likely explanation is that the experimental procedures were slightly different: in the screening assay, the cells were infected with virus at a multiplicity of infection (MOI) of 0.001, while in this validation assay, the MOI was 0.01. To further demonstrate the antiviral activity of TMEM45B, we monitored the viral replication with or without TMEM45B overexpression in 293T cells. The cells were challenged with the virus. At different time points postinfection, aliquots of culture supernatants were collected to infect BHK-21 cells, which were later lysed to measure the luciferase activity. In the culture supernatants of the control 293T cells, the relative virus titer, as indicated by nLuc activity in the BHK-21 cells, increased over time (Fig. 1C), reflecting the replication of the reporter virus. In contrast, in the culture supernatants of the NZAP-Zeo- and TMEM45B-expressing cells, the virus titer barely increased (Fig. 1C). These results indicate that TMEM45B overexpression inhibits SINV replication.

To test whether the endogenous TMEM45B is active against the virus, two small interfering RNAs (siRNAs) targeting different sites of TMEM45B were transfected into 293A cells to downregulate the expression of the endogenous TMEM45B. In the cells in which TMEM45B expression was downregulated, the viral replication was significantly enhanced (Fig. 1D). These results indicated that TMEM45B inhibits SINV replication at the endogenous level.

To probe whether the antiviral activity of TMEM45B is specific to SINV, we analyzed the effect of its overexpression on the replication of influenza A virus (IAV). While NZAP-Zeo inhibited the viral replication, as reported previously (59), overexpression of TMEM45B had no effect on IAV replication (Fig. 1E). These results indicate that the antiviral activity of TMEM45B against SINV was not caused by nonspecific toxicity to the cells.

TMEM45B is localized mainly in the endosomes, lysosomes, and *trans*-Golgi network. To explore how TMEM45B inhibits SINV replication, we first analyzed its cellular localization in BHK or 293T cells. Very similar results were obtained, and the results with 293T cells are presented in Fig. 2A. Myc-tagged TMEM45B was coexpressed with red fluorescent protein-tagged organelle markers, and the protein localizations were

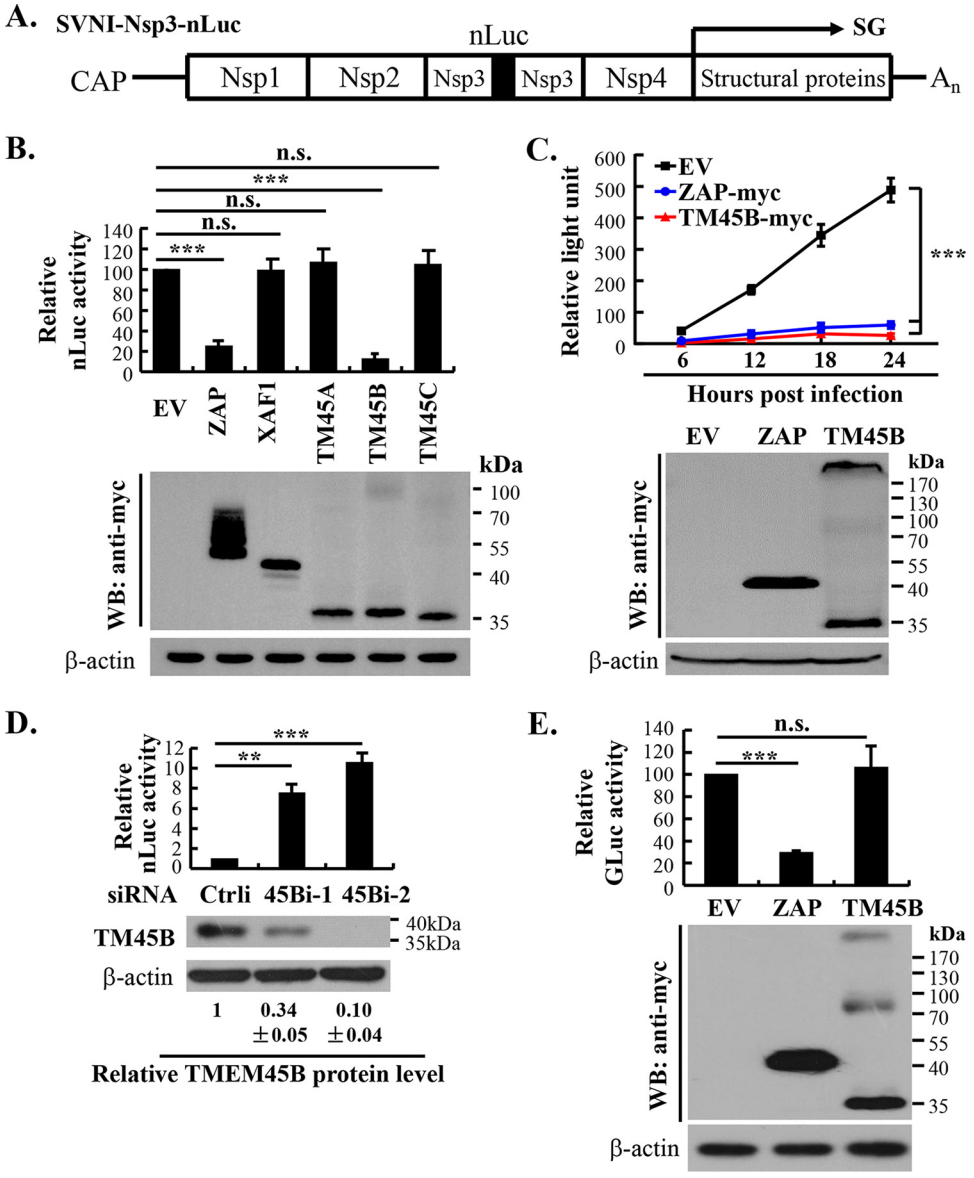

FIG 1 TMEM45B inhibits SINV replication. (A) Schematic representation of SVNI-Nsp3-nLuc. The nLuc reporter was expressed in fusion with split Nsp3. SG, subgenomic RNA. (B) 293T cells were transfected with plasmids expressing the proteins indicated. At 48 h posttransfection, the cells were infected with SVNI-Nsp3-nLuc at an MOI of 0.01 PFU/cell. At 24 h postinfection, the cells were analyzed for luciferase activity (upper panel). Protein expressions were confirmed by Western blotting (WB; lower panel). EV, empty vector; TM45A, TMEM45A-myc; TM45B, TMEM45B-myc; TM45C, TMEM45C-myc; ZAP-myc, NZAP-Zeo-myc, to serve as a positive control; XAF1, XAF1-myc, an ISG product to serve as a negative control. (C) 293T cells were transfected with plasmids expressing the proteins indicated. At 48 h posttransfection, the cells were infected with SVNI-Nsp3-nLuc at an MOI of 0.01 PFU/cell. At different time points postinfection, aliquots of culture supernatants were collected to infect BHK-21 cells, which were later lysed to measure the luciferase activity as an indicator of the relative amount of the virus in the culture supernatant of the 293T cells (upper panel). Protein expressions were confirmed by Western blotting (lower panel). (D) 293A cells were transfected with the siRNAs indicated. At 48 h posttransfection, the cells were infected with SVNI-Nsp3-nLuc at an MOI of 0.01 PFU/cell. At 48 h postinfection, the cells were analyzed for protein levels and luciferase activity. The intensities of the bands of TMEM45B were determined by ImageJ and normalized to those of β-actin. The relative protein level of TMEM45B, as indicated by the normalized intensity, in the control cells was set as 1. Data presented are means ± SD of the results of three independent experiments. Ctrli, control siRNA; 45 Bi-1 and 45 Bi-2, siRNAs targeting different sites of TMEM45B. (E) 293T cells were transfected with plasmids expressing the proteins indicated. At 48 h posttransfection, the cells were infected with IAV-Gluc at an MOI of 0.01 PFU/cell. At 24 h postinfection, cells were analyzed for luciferase activity (upper panel). The relative luciferase activity in the control cells was set as 100. Protein expressions were confirmed by Western blotting (lower panel). Data presented are means ± SD of the results of three independent experiments. **, $P < 0.01$; ***, $P < 0.001$; n.s., $P > 0.05$.

TABLE 1 ISGs screened to inhibit SVNI-Nsp3-nLuc production[a]

Gene name	Fold inhibition
Empty vector	1
TMEM45B	46.081
TMEM217	12.371
BCL2A1	11.330
AGPAT4	7.860
ZAP	5.945
TMEM106A	5.890
ASPHD2	5.500
SEMA4G	5.495
IFI27	4.830
EVL	4.752
GLYATL1	4.742
ST3GAL5	3.808
RTP4	3.723
ITGB7	3.657
CKB	3.655
NPC2	3.559
EPSTI1	3.526
CD36	3.453
TRIM31	3.339
TKTL1	2.967
ETV4	2.724
SLAMF8	2.681
FNDC5	2.566
DCLRE1C	2.514
INPP1	2.487
IFI44	2.449
LMO2	2.448
FTSJD2	2.391
GPR84	2.380
GSDMD	2.373
NAPSA	2.366
RNF213	2.361
FAM122C	2.326
DDX60L	2.257
SELL	2.119
SP140L	1.989
MOXD1	1.976
ENTPD1	1.908
USP18	1.887
FRMD3	1.828
BFSP2	1.780
TPPP2	1.776
TOR1B	1.762
MS4A12	1.741
CHI3L2	1.650
BOC	1.639
MR1	1.615
ENDOD1	1.614
GALM	1.606
C1orf38	1.583
REC8	1.575
CXorf21	1.558
CCDC146	1.519
APOL6	1.484
MYO5C	1.421
IFI6	1.414
RASGRP3	1.357
LGALS3BP	1.329
ECE1	1.322
IFIT5	1.318
TMEM140	1.298

(Continued on next page)

TABLE 1 (Continued)

Gene name	Fold inhibition
LHFPL1	1.268
PARP3	1.239
MGC87042	1.239
ARHGAP25	1.152
B3GNT2	1.111
PDS5A	1.087
GBP4	1.077
MFN1	0.990
XAF1	0.983
CD69	0.903
TIPARP	0.894
TEAD4	0.863
NPHP1	0.853
FCGR2C	0.853
IFI44L	0.830
CFLAR	0.808
NFKBIE	0.707
CASP10	0.667
PHLDA2	0.643
CREM	0.631
C20orf103	0.619
PDE6H	0.616
FAM109B	0.594
XRN2	0.578
DDAH2	0.557
IDH1	0.555
WDFY1	0.508
RNASET2	0.471
GSN	0.411
MVP	0.401
C14orf149	0.394
AZU1	0.374
MSMB	0.349
SNX9	0.321
EGR1	0.305
NAT8L	0.299
PIM1	0.295
BRWD1	0.291
RNF149	0.287
PLAC8	0.269
RUNX3	0.219
FGD2	0.174
TIMD4	0.117

[a]The ISGs were cloned into a protein expression vector and transiently expressed in 293T cells, followed by infection of the cells with the reporter virus SVNI-Nsp3-nLuc at an MOI of 0.001 for 1 h. At 24 h postinfection, the nLuc activity in the infected cells was measured and used as an indicator of the viral replication. Fold inhibition was calculated as the luciferase activity in the control cells divided by that in the ISG-expressing cells. The zinc finger antiviral protein (ZAP) was used as a positive control.

analyzed by immunostaining imaging. TMEM45B was well colocalized with TGN38 (*trans*-Golgi marker), Rab5 (early endosome marker), Rab7 (late endosome marker), and Lamp1 (late endosome/lysosome marker) (Fig. 2A). In comparison, the distribution pattern of TMEM45B was quite different from that of the endoplasmic reticulum (ER) marker DsRed2-ER (Fig. 2A). In addition, no obvious TMEM45B expression at the plasma membrane was detected (Fig. 2A).

We next tried to analyze whether the endogenous TMEM45B is localized in the endosome/lysosome. The anti-TMEM45B antibody failed to detect the endogenous protein in the immunostaining imaging assay in our hands. We thus employed the cell lysate fractionation assay. 293T cells were lysed, and the cell lysate was fractionated using discontinuous iodixanol gradient centrifugation (60). The distribution pattern of the endogenous TMEM45B overlapped that of the endosome/lysosome marker Lamp1

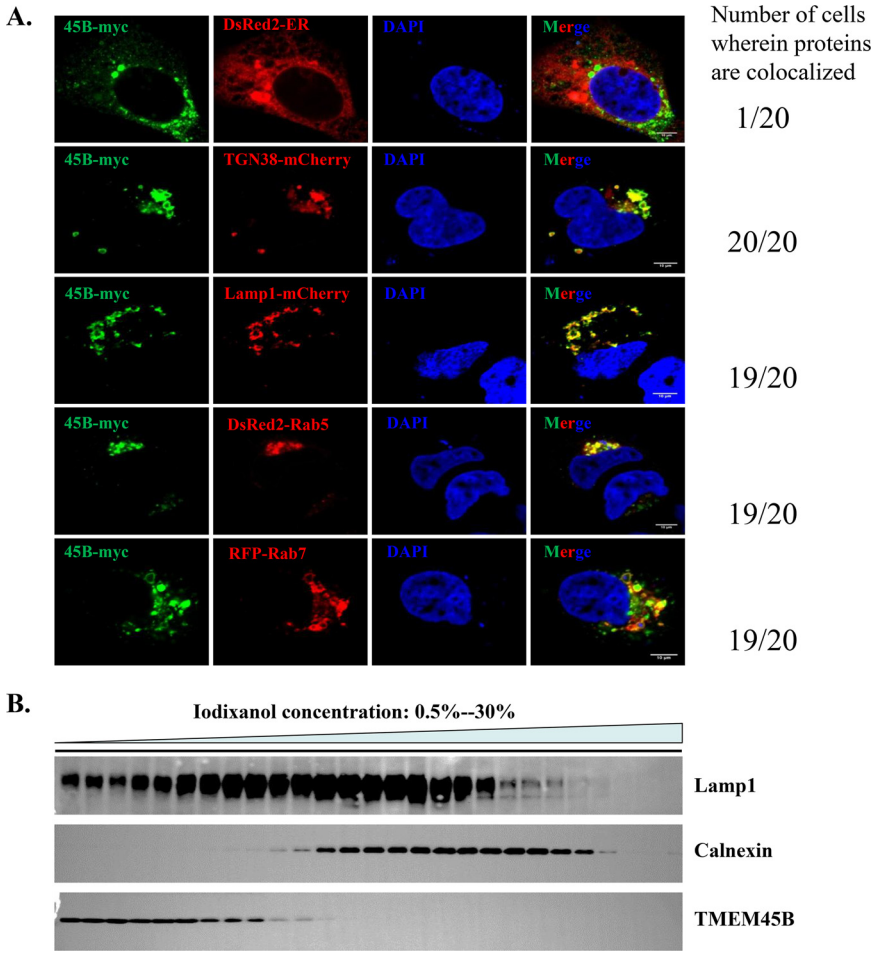

FIG 2 Intracellular localization of TMEM45B. (A) 293T cells were transfected with a plasmid expressing TMEM45B-myc, together with a plasmid expressing an organelle marker fused with a red fluorescent protein. At 16 h posttransfection, the cells were fixed in paraformaldehyde. TMEM45B-myc was stained with anti-myc antibody and Alexa 488-conjugated secondary antibody (green). Fluorescence images were obtained by confocal fluorescence microscopy (left). Scale bar, 10 μm. Twenty randomly selected cells were analyzed to determine the colocalization of TMEM45B with the organelle marker (right). 45B, TMEM45B. Data presented are representative of three independent experiments. (B) The lysate of 293T cells was fractionated through iodixanol gradients as described in Materials and Methods. The cell lysate fractions were subjected to Western blotting to analyze the distribution patterns of the endogenous proteins indicated. Lamp1, marker for late endosome/lysosome; calnexin, marker for ER. Data presented are representative of three independent experiments.

but not that of the ER marker calnexin (Fig. 2B). These results are consistent with the above-described imaging results.

TMEM45B interacts with Nsp1 and Nsp4. In attempt to understand how TMEM45B inhibits SINV replication, we analyzed whether it interacts with the viral nonstructural proteins. Myc-tagged TMEM45B was coexpressed with a Flag-tagged nonstructural protein, and the interaction was analyzed by coimmunoprecipitation assays. Immunoprecipitation of Nsp1 or Nsp4 coprecipitated TMEM45B (Fig. 3A). In contrast, immunoprecipitation of Nsp2 or Nsp3 failed to do so (Fig. 3A). We next tested whether endogenous TMEM45B interacts with Nsp1 or Nsp4. Since we did not have an antibody against Nsp1 or Nsp4, we engineered the SVNI-Nsp3-nLuc virus to tag Nsp1 with a Flag tag at the N terminus. 293T cells were infected with the engineered virus (SVNI-Flag-Nsp1) (Fig. 3B). Immunoprecipitation of Flag-Nsp1 coprecipitated endogenous TMEM45B (Fig. 3C), indicating that endogenous TMEM45B interacts with Nsp1.

To further show the interactions between TMEM45B and Nsp1 and Nsp4, we employed

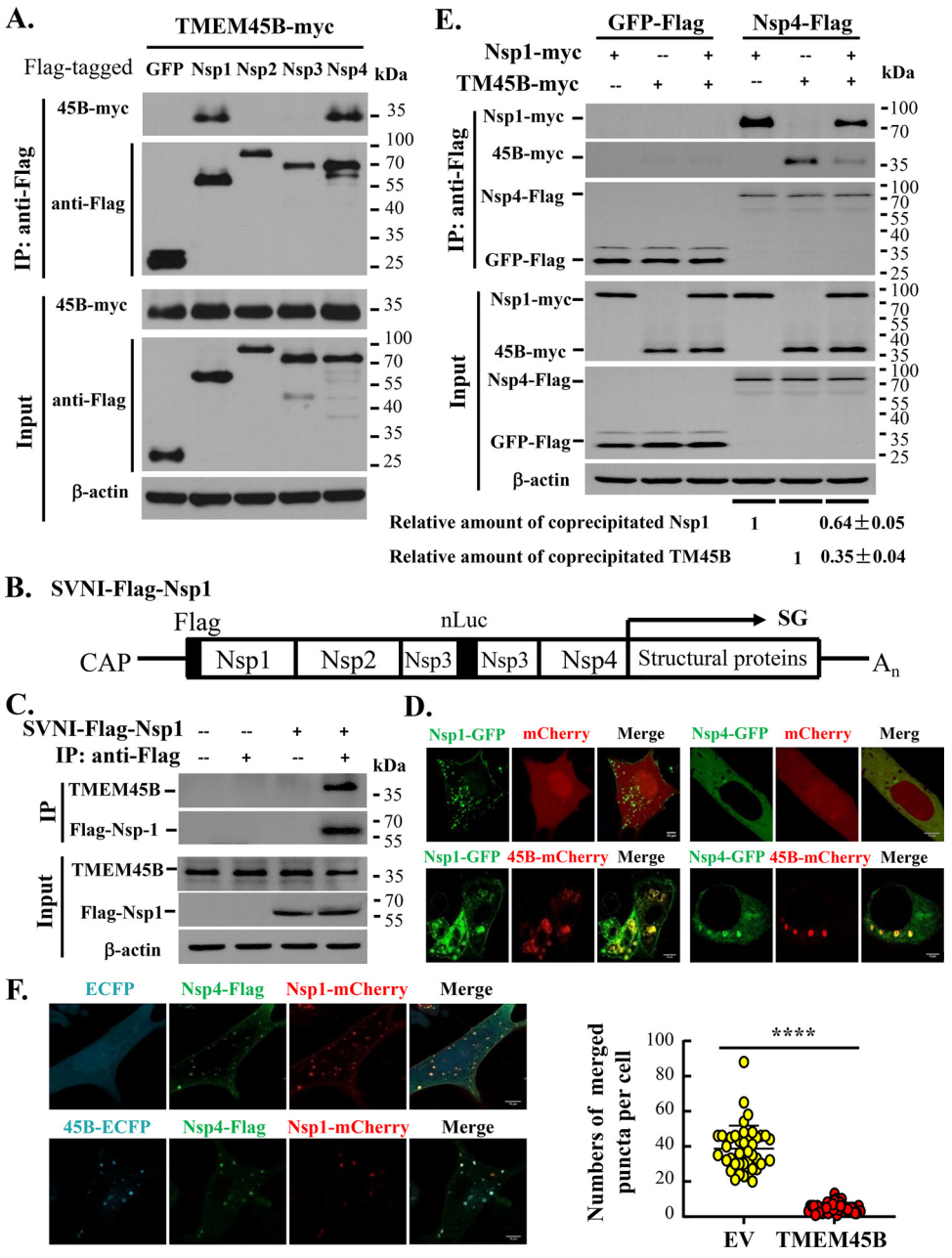

FIG 3 TMEM45B interacts with Nsp1 and Nsp4. (A) Flag-tagged Nsp1, Nsp2, Nsp3, Nsp4, or GFP was transiently coexpressed with TMEM45B-myc in 293T cells. At 48 h posttransfection, cell lysates were immunoprecipitated (IP) with Anti-Flag affinity gel, and the precipitated proteins were analyzed by Western blotting. (B) Schematic representation of SVNI-Flag-Nsp1. SG, subgenomic RNA. (C) 293T cells were infected with SVNI-Flag-Nsp1 at an MOI of 20 PFU/cell for 6 h at 37°C. After extensive washing, the cells were lysed and immunoprecipitated with Anti-Flag affinity gel or control IgG. The precipitated proteins were analyzed by Western blotting. (D) The proteins indicated were transiently coexpressed in BHK-21 cells. At 16 h posttransfection, the cells were fixed with paraformaldehyde and analyzed by confocal fluorescence microscopy. Scale bar, 10 μm. (E) Myc-tagged Nsp1 and TMEM45B were either individually expressed or coexpressed together with Flag-tagged Nsp4 or GFP in 293T cells. At 48 h posttransfection, the cells were lysed and immunoprecipitated with Anti-Flag affinity gel. The precipitated proteins were analyzed by Western blotting. The intensities of the bands of Nsp1 or TMEM45B were determined by ImageJ and normalized to those of β-actin. The relative amount of coprecipitated Nsp1 or TMEM45B was calculated. Data presented are means ± SD of the results of three independent experiments. (F) Plasmids expressing the proteins indicated were transiently cotransfected into BHK-21 cells. At 16 h posttransfection, the cells were fixed. Nsp4-Flag was detected with anti-Flag antibody and Alexa 488-conjugated secondary antibody. The cells were analyzed by confocal fluorescence microscopy (left). Scale bar, 10 μm. The numbers of puncta with merged Nsp1 and Nsp4 signals were counted in 40 randomly selected cells (right). Data presented are means ± standard errors of the mean (SEM) of the numbers of puncta with merged signals. ****, $P < 0.0001$. 45B, TMEM45B.

confocal microscopy. TMEM45B was fused with the red fluorescent protein mCherry at the C terminus, and Nsp1 or Nsp4 was fused with green fluorescent protein (GFP). The proteins were transiently coexpressed in BHK-21 cells. When coexpressed with the control protein mCherry, Nsp1 was detected at the plasma membrane and puncta in the cytoplasm (Fig. 3D). When coexpressed with TMEM45B-mCherry, Nsp1 was also detected at the plasma membrane and puncta in the cytoplasm, but the puncta appeared to be larger than those in the cells without TMEM45B-mCherry (Fig. 3D). Obvious colocalization of Nsp1 with TMEM45B-mCherry was observed in the cytoplasm but not at the plasma membrane (Fig. 3D). When Nsp4 was coexpressed with mCherry, it was distributed throughout the cytoplasm (Fig. 3D). However, when coexpressed with TMEM45B-mCherry, Nsp4 colocalization with TMEM45B-mCherry to punctate structures was obvious (Fig. 3D). These results further supported the interactions of TMEM45B with Nsp1 and Nsp4.

As key components of the replication complex, Nsp1 and Nsp4 interact with each other (61). Given that TMEM45B interacts with both Nsp1 and Nsp4, we speculated that TMEM45B might interfere with the interaction between Nsp1 and Nsp4. To test this idea, we analyzed the interaction between Nsp1 and Nsp4 with or without TMEM45B. In the coimmunoprecipitation assay, TMEM45B reproducibly and significantly reduced the interaction (Fig. 3E). Consistently, the presence of Nsp1 reduced the interaction of TMEM45B with Nsp4 (Fig. 3E). We also employed confocal microscopy to analyze whether TMEM45B interferes with the interaction between Nsp1 and Nsp4. TMEM45B was fused with enhanced cyan fluorescent protein (ECFP) at the C terminus, Nsp1 was fused with mCherry, and Nsp4 was Flag tagged at the C terminus. The proteins were transiently coexpressed in BHK-21 cells. When coexpressed with the control protein ECFP, obvious colocalization of Nsp1 with Nsp4 was observed in the cytoplasm (Fig. 3F, left upper panels). In comparison, when coexpressed with TMEM45B-ECFP, Nsp1 colocalization with Nsp4 to punctate structures was substantially reduced (Fig. 3F, left lower panels). Statistical analysis of the cells showed that the numbers of merged puncta per cell reduced dramatically in the presence of TMEM45B (Fig. 3F, right). These results further support the notion that TMEM45B interferes with the interaction between Nsp1 and Nsp4.

TMEM45B reduces the protein level expressed from the viral RNA. The foregoing results revealed that TMEM45B is localized mainly in endosomes, lysosomes, and the *trans*-Golgi network but not obviously at the plasma membrane and that TMEM45B interacts with Nsp1 and Nsp4. We thus speculated that TMEM45B might not inhibit virus binding to the cells. Given that the viral RNA is associated with Nsp1, which is crucial for the capping of newly synthesized viral RNA, the interaction of TMEM45B with Nsp1 might interfere with the association of Nsp1 with SINV genomic RNA or with its capping activity. We thus speculated that TMEM45B might affect the viral protein expression through inhibition of viral RNA translation or promotion of viral RNA destabilization. In addition, the interaction of TMEM45B with Nsp1 and Nsp4 suggested that it might interfere with the function of the replication complex.

To examine whether TMEM45B inhibits virus binding, TMEM45B knockdown and control 293A cells were incubated with the SVNI-Nsp3-nLuc virus at 4°C to allow binding without penetration. After extensive washing to remove the unbound virus, the amount of the cell-associated viral RNA was measured. No difference was detected between the TMEM45B knockdown and control cells (Fig. 4B and C), suggesting that TMEM45B downregulation did not affect virus binding to the cells. These results are consistent with the observations above that TMEM45B was barely detected at the plasma membrane.

We next transfected the viral RNA generated by *in vitro* transcription to bypass the virus entry step and analyzed the effect of TMEM45B on viral protein synthesis. The mutant SINV reporter SINV-Nsp3-nLuc-Pol$^-$ was used. In this SINV strain Toto1101-based reporter, the nLuc coding sequence was inserted into Nsp3 such that nLuc is expressed in frame with Nsp3, and a fragment of Nsp4 was deleted to abolish the enzymatic activity of the RNA-dependent RNA polymerase (Fig. 4A). The 5′-capped viral RNA and control firefly luciferase-encoding RNA were generated by *in*

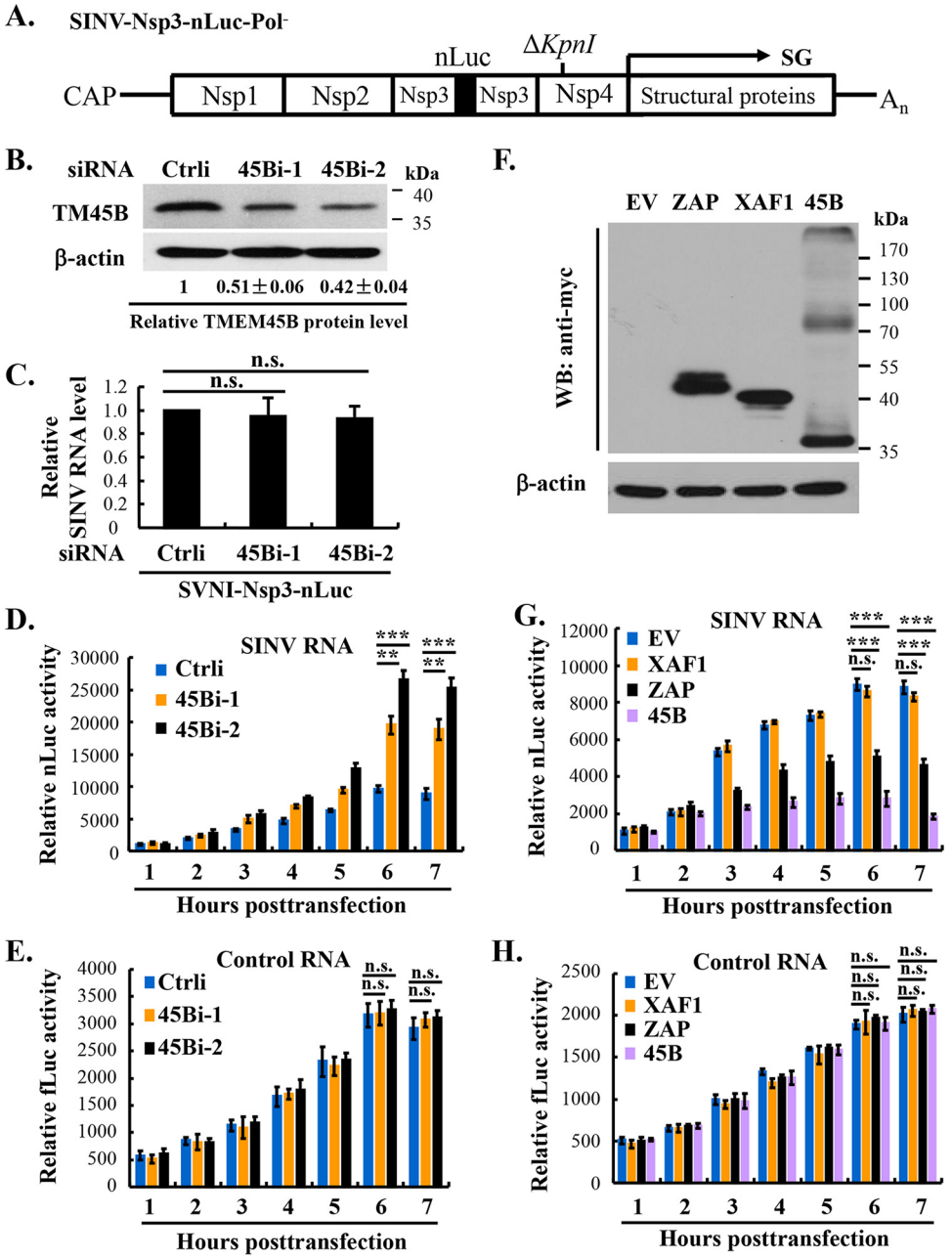

FIG 4 TMEM45B inhibits SINV infection at a step after entry. (A) Schematic representation of nLuc-expressing SINV-Nsp3-nLuc-Pol$^-$. The 36-nucleotide deletion (ΔKpnI) in the coding sequence of Nsp4 of SINV strain Toto1101 resulted in a defective RNA-dependent RNA polymerase. SG, subgenomic RNA. (B) 293A cells were transfected with the siRNAs indicated, and the downregulation of TMEM45B was confirmed by Western analysis, as described in the legend to Fig. 1D. (C) The cells were incubated with SVNI-Nsp3-nLuc (10 PFU/cell) for 1 h at 4°C to allow binding without penetration of the virus. The cells were washed extensively, and the cell-associated viral RNA level was measured. (D and E) The cells as described for panel B were transfected with a mixture of *in vitro*-transcribed and capped SINV-Nsp3-nLuc-Pol$^-$ RNA and firefly luciferase-encoding control RNA. At the time points indicated, the cells were analyzed for luciferase activities. (F to H) 293T cells were transfected with plasmids expressing the proteins indicated. At 48 h posttransfection, the cells were transfected with a mixture of the SINV-Nsp3-nLuc-Pol$^-$ RNA and firefly luciferase-encoding control RNA. At the time points indicated, the cells were analyzed for protein expressions (F) and luciferase activities (G and H). EV, empty vector; ZAP and XAF1, controls as described in the legend to Fig. 1B; 45B, TMEM45B-myc. Data presented are means ± SD of the results of three independent experiments. **, $P < 0.01$; ***, $P < 0.001$; n.s., $P > 0.05$.

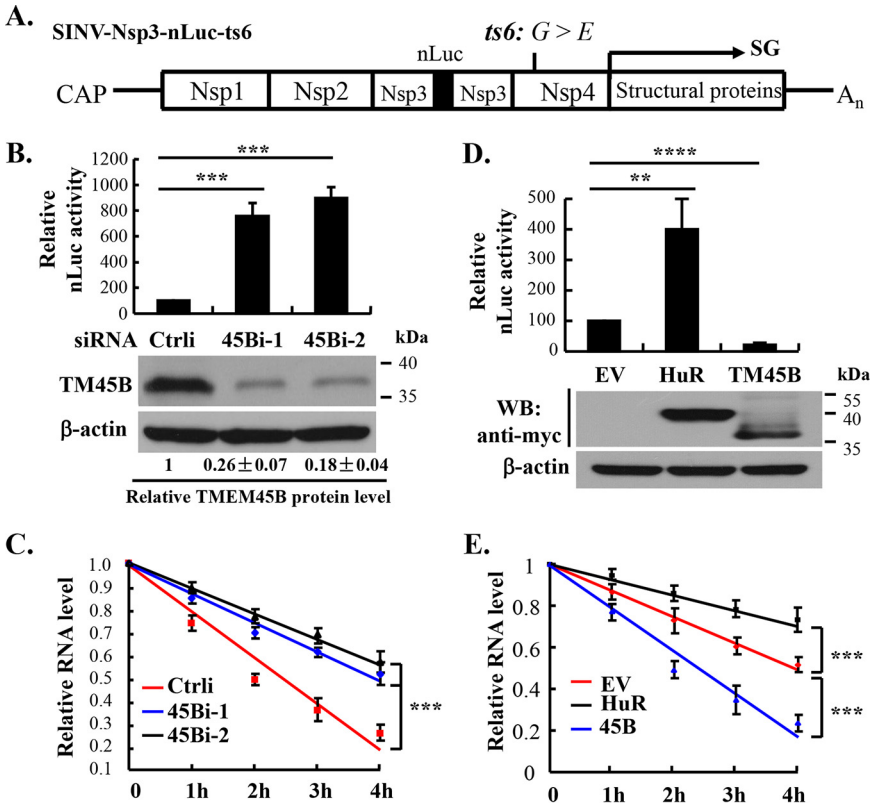

FIG 5 TMEM45B promotes SINV RNA degradation. (A) Schematic representation of SINV-Nsp3-nLuc-ts6. The Gly-to-Glu mutation in Nsp4 of SINV strain Toto1101 rendered the virus temperature sensitive: the virus can replicate at 28°C but not at 40°C. SG, subgenomic RNA. (B to E) Cells were transfected with the siRNAs (B and C) or plasmids (D and E) indicated. At 48 h posttransfection, the cells were incubated with SINV-Nsp3-nLuc-ts6 virus at an MOI of 20 PFU/cell for 1 h at 4°C. (B and D) The cells were shifted to 28°C and cultured for 24 h, followed by measurement of the luciferase activity and protein expression levels. The relative TMEM45B level was determined as described in the legend to Fig. 1D. (C and E) The cells were shifted to 40°C. At the time points indicated, the cells were lysed and the viral RNA levels were measured. Data presented are means ± SD of the results of three independent experiments. **, $P < 0.01$; ***, $P < 0.001$; ****, $P < 0.0001$; n.s., $P > 0.05$.

vitro transcription and transfected into the TMEM45B knockdown 293A cells. At various time points posttransfection, luciferase activities were measured. Downregulation of TMEM45B increased the nLuc activity expressed from the viral RNA (Fig. 4D). In contrast, the firefly luciferase activity expressed from the control RNA was little affected (Fig. 4E). To potentiate these results, TMEM45B was overexpressed in 293T cells (Fig. 4F). NZAP-Zeo, which inhibits the expression of the viral proteins by inhibiting the translation and promoting the degradation of SINV RNA (44), was used as a positive control, and XAF1 was used as a negative control (Fig. 4F). In line with the above-described results, overexpression of TMEM45B inhibited luciferase expression from the viral reporter RNA (Fig. 4G) but had little effect on the control reporter RNA (Fig. 4H). These results indicate that TMEM45B inhibits SINV infection at a step after virus entry and suggested that TMEM45B inhibits the expression of the viral protein from the viral RNA.

TMEM45B promotes SINV RNA degradation. We next set to explore whether TMEM45B affects the stability of the viral RNA. We first tested the effect of downregulation of endogenous TMEM45B on the stability of the viral RNA. 293A cells in duplicate dishes were transfected with a control siRNA or the siRNAs targeting TMEM45B and then infected with SINV-Nsp3-nLuc-ts6 at 4°C for 1 h. In this SINV strain Toto1101-based reporter, the nLuc coding sequence was inserted into Nsp3 such that nLuc was expressed in frame with Nsp3, and a mutation was introduced into Nsp4 to make the RNA-dependent RNA

polymerase enzymatic activity temperature sensitive (Fig. 5A). The virus replicates at the permissive temperature (28°C) but not at the nonpermissive temperature (40°C) (62). One dish of the cells was cultured at the permissive temperature to confirm that downregulation of TMEM45B enhanced the viral infection (Fig. 5B). The other dish of cells was switched to the nonpermissive temperature to prevent viral RNA amplification. At different time points postinfection, the viral RNA levels were measured. The results showed that downregulation of TMEM45B increased the stability of the viral RNA (Fig. 5C). To substantiate these results, TMEM45B was overexpressed in 293T cells. HuR was used as a control, which was reported to stabilize SINV RNA (63). As expected, overexpression of TMEM45B inhibited and HuR enhanced SINV infection (Fig. 5D). In line with the above-described results, TMEM45B overexpression reduced the stability of SINV RNA, while overexpression of HuR enhanced the stability of the viral RNA (Fig. 5E).

TMEM45B renders membrane-associated SINV RNA sensitive to RNase A treatment. As a viral RNA capping enzyme and the membrane anchor of the SINV replication complex (12, 64), Nsp1 is associated with the viral RNA. The foregoing results suggested that TMEM45B might disrupt the viral replication complex. Hence, one would expect that TMEM45B might also interfere with the interaction of the viral RNA with Nsp1. To test this possibility, we analyzed the association of the viral RNA with Nsp1 with or without TMEM45B. 293T cells were transiently transfected with an empty vector or a plasmid expressing TMEM45B-myc, followed by infection with the SVNI-Flag-Nsp1 virus. At 6 h postinfection, the cells were lysed. Under this condition, TMEM45B did not significantly affect the viral RNA levels (Fig. 6A, left). The cell lysate was immunoprecipitated with control IgG or anti-Flag antibody, and the amount of associated viral RNA was measured. In the absence of TMEM45B, the viral RNA was enriched by the anti-Flag antibody but not by the control IgG (Fig. 6A, middle). In contrast, in the presence of TMEM45B, little enrichment was observed (Fig. 6A, middle). TMEM45B did not affect the amount of Nsp1 immunoprecipitated by the anti-Flag antibody (Fig. 6A, right). These results indicate that TMEM45B interferes with the interaction of the viral RNA with Nsp1.

The viral replication complex of SINV is believed to be associated with the intracellular membrane for protection from cellular defense mechanisms. The above-described results suggested that TMEM45B might deprive the viral RNA of the protection. To test this hypothesis, we analyzed the sensitivity of the membrane-associated viral RNA to RNase A treatment. 293T cells were transfected with a plasmid expressing myc-tagged TMEM45B and a control plasmid expressing *Renilla* luciferase-encoding mRNA, followed by infection with SVNI-Nsp3-nLuc. At 1.5 h postinfection, the cells were lysed, the cell lysate was fractionated, and the postnuclear supernatant (PNS) was subjected to a membrane flotation assay (Fig. 6B). In this assay, the PNS was mixed with 85% sucrose to a final concentration of 73%. On top of the PNS was layered 65% and 10% sucrose. After centrifugation, the membrane and associated molecules (including proteins and nucleic acids) are expected to float up to the interface of 65% and 10% sucrose, and the nonmembrane-associated proteins are expected to stay in the 73% sucrose, with some diffusion into the 65% sucrose. Twelve fractions were collected, with fraction 3 containing the membranes and associated molecules. The fractionated lysates were treated with RNase A, followed by measurement of the RNA levels by quantitative reverse transcription-PCR (RT-qPCR). TMEM45B was detected mainly in fraction 3, while GFP was detected mainly in fractions 9 to 11, the nonmembrane fractions (Fig. 6C). The ribosomal protein S16 was detected in both the membrane and nonmembrane fractions (Fig. 6C). Overexpression of TMEM45B did not obviously affect the distribution pattern of the viral RNA, which was detected in both membrane and nonmembrane fractions (Fig. 6D, compare the red and blue bars). In the absence of TMEM45B, RNase A treatment of the membrane fraction had little effect on the viral RNA (Fig. 6D, compare the red and orange bars in fraction 3), while in the nonmembrane fractions, RNase A treatment significantly reduced the viral RNA levels (Fig. 6D, compare the red and orange bars in fractions 8 to 11). In the presence of TMEM45B, RNase A treatment of the membrane fraction dramatically reduced the viral RNA

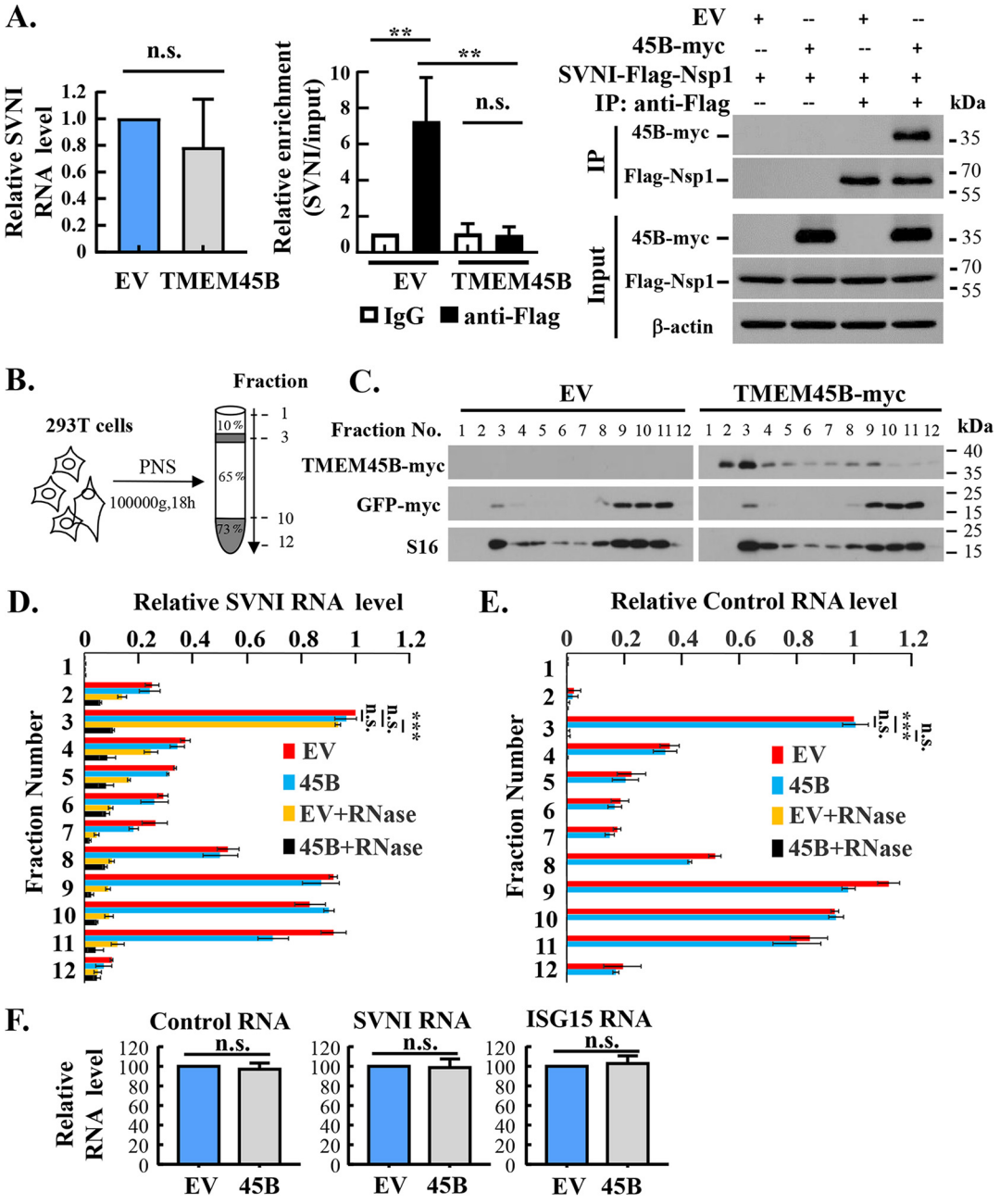

FIG 6 TMEM45B renders membrane-associated SINV RNA sensitive to RNase A treatment. (A) TMEM45B inhibits the interaction of the viral RNA with Nsp1. 293T cells were transfected with an empty vector or a plasmid expressing TMEM45B-myc. At 48 h posttransfection, the cells were infected with SVNI-Flag-Nsp1 at an MOI of 20 PFU/cell for 6 h at 37°C. After extensive washing, the cells were lysed. The viral RNA levels in the cell lysate were measured (left). The cell lysate was immunoprecipitated with Anti-Flag affinity gel or control IgG. Association of the viral RNA with Nsp1 or IgG was indicated by relative enrichment, which was calculated as the amount of the viral RNA in the precipitates divided by that in the input cell lysate. The relative enrichment of the viral RNA immunoprecipitated with control IgG in the cells expressing empty vector was set as 1 (middle). Precipitated proteins were analyzed by Western blotting (right). Data presented are means ± SD of the results of three independent experiments. (B) Schematic illustration of the experimental procedure. 293T cells were transfected with an empty vector or a plasmid expressing TMEM45B-myc. Plasmids expressing *Renilla* luciferase and GFP-myc were included to serve as controls. At 48 h posttransfection, the cells were infected with SVNI-Nsp3-nLuc at an MOI of 20 PFU/cell for 1.5 h at 37°C. After extensive washing, the cells were lysed in hypotonic buffer and the lysates were centrifuged. The postnuclear supernatant (PNS) was analyzed by the membrane flotation assay (see Materials and Methods for details). (C) Protein levels in each fraction were analyzed by Western blotting. S16, a ribosomal protein. (D and E) PNS was subjected to the membrane flotation assay, and fractions were collected. One aliquot of each fraction was treated with RNase A. The RNA in the samples with or without RNase A treatment was extracted and quantitated. The relative RNA level in fraction 3 of the cells transfected with the empty vector was set as 1. Control RNA, the *Renilla* luciferase-encoding RNA expressed from the transfected plasmid. (F) The levels of the control RNA, SVNI RNA, and ISG15 RNA in PNS were measured. The relative RNA level in the empty vector-transfected cells was set as 100. Data presented are means ± SD of the results of two independent experiments. **, $P < 0.01$; ***, $P < 0.001$; n.s., $P > 0.05$. 45B, TMEM45B.

levels (Fig. 6D, compare the orange and black bars in fraction 3). The viral RNA in the nonmembrane fractions was not protected with or without TMEM45B (Fig. 6D, compare orange and black bars in fractions 8 to 11). The control *Renilla* luciferase-encoding mRNA was sensitive to RNase A treatment in both the membrane and nonmembrane fractions (Fig. 6E). TMEM45B did not significantly affect the total amount of the viral RNA or the control RNA in the PNS (Fig. 6F). These results are consistent with the notion that SINV RNA is protected by the intracellular membranes and that TMEM45B overexpression deprived the viral RNA of this protection. To test whether the exposed viral RNA would trigger an innate immune response, we analyzed the ISG15 RNA levels. No obvious difference was observed with or without TMEM45B (Fig. 6F).

The formation of SINV-induced cytopathic vacuoles is diminished in TMEM45B-expressing cells. The amplification of the viral replication complex leads to the formation of virus-induced cytopathic vacuoles. To explore whether TMEM45B affects this process, the TMEM45B-expressing cells were infected with a replication-competent SINV carrying GFP and the localization of the viral replication complex was monitored over the course of infection. It was previously established that the newly synthesized viral protein Nsp3 colocalizes with the double-stranded viral RNA (dsRNA), a hallmark of the viral replication complex (11). To detect the replication complex, GFP was expressed in fusion with Nsp3 (Fig. 7A) in SVNI, resulting in the replication-competent virus SVNI-Nsp3-GFP, a strategy adapted from the above-mentioned studies. The GFP insertion had only a minor effect on the viral replication and allowed us to monitor the virus-specific protein complex using fluorescence microscopy.

BHK-21 cells were transfected with a plasmid expressing mCherry or TMEM45B-mCherry. The cells were incubated with SVNI-Nsp3-GFP at an MOI of 500 PFU/cell for 1 h at 4°C to allow virus binding without penetration and then shifted to 37°C. At different time points postinfection, the cells were fixed and analyzed by confocal microscopy. Consistent with the previously reported results, in the control cells, GFP was first detected at the plasma membrane at 1.5 h postinfection (Fig. 7B). At 2.5 h postinfection, GFP was detected in the cytoplasm diffusing from the plasma membrane, and at 4 h postinfection, GFP was detected in vesicles throughout the cytoplasm (Fig. 7B). In the TMEM45B-expressing cells, GFP was also detected at the plasma membrane at the early stage of infection (Fig. 7B). We noticed that the GFP signal at 1.5 h postinfection in the TMEM45B-expressing cells was only slightly weaker than that in the control cells. However, at later stages of infection, GFP was barely detected in the cytoplasm (Fig. 7B). For better resolution of the GFP signals, structure illumination (SIM) ultra-high-resolution fluorescence microscopy was employed. At 1.5 h postinfection, GFP signals were detected in clusters at the plasma membrane with or without TMEM45B (Fig. 7C). In the control cells, larger vesicles were seen in the cytoplasm at 2.5 h postinfection, and cytopathic vacuoles (CPV) of about 200 nm were observed at 4 h postinfection (Fig. 7C). In the TMEM45B-expressing cells, GFP was observed only at the plasma membrane (Fig. 7C). Quantitative analysis of multiple randomly selected GFP-positive cells revealed that more than 90% of the cells had GFP signals at the plasma membrane at 1.5 h postinfecton, with or without TMEM45B (Fig. 7D). This percentage did not change much over time for the TMEM45B-expressing cells. However, for the control cells, nearly 90% of the cells had strong GFP signals in the cytoplasm in the later stages of infection (Fig. 7D). These results indicate that under this experimental condition, TMEM45B had little effect on the localization of the viral proteins at the plasma membrane. However, the formation of CPVs in the cytoplasm was significantly diminished in TMEM45B-expressing cells (see below for further discussion). The colocalization of Nsp3-GFP with the viral dsRNA was also analyzed (Fig. 7E). BHK-21 cells were transfected with a plasmid expressing mCherry or TMEM45B-mCherry, followed by infection with the SVNI-Nsp3-GFP virus. At 6 h postinfection, cells were fixed, stained with anti-dsRNA antibody, and analyzed by confocal microscopy. The dsRNA signals colocalized well with the GFP signals (Fig. 7E). Consistent with the above-described results, in the absence of TMEM45B, nearly 90% of the cells had strong GFP and dsRNA signals in the cytoplasm (Fig. 7E and F). In contrast, in the presence of TMEM45B, the GFP and dsRNA signals were detected mainly at the plasma membrane (Fig. 7E and F).

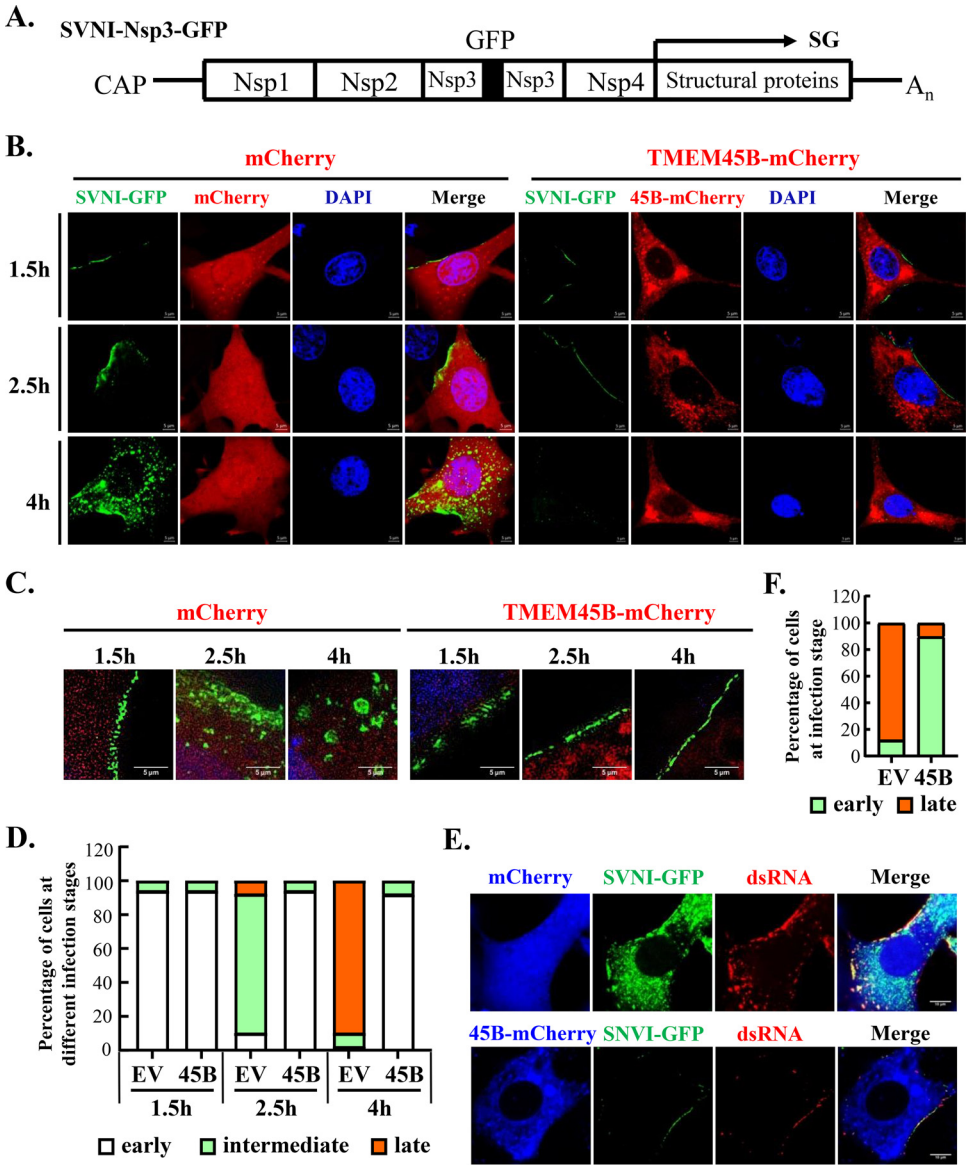

FIG 7 The formation of SINV-induced cytopathic vacuoles is diminished in TMEM45B-expressing cells. (A) Schematic representation of GFP-expressing virus SVNI-Nsp3-GFP. SG, subgenomic RNA. (B to D) BHK-21 cells were transfected with a plasmid expressing mCherry or TMEM45B-mCherry. At 24 h posttransfection, the cells were incubated with SVNI-Nsp3-GFP at an MOI of 500 PFU/cell at 4°C for 1 h and then shifted to 37°C. At the time points indicated, the cells were fixed and analyzed by confocal fluorescence microscopy or structure illumination microscopy. (B) Confocal microscopy analysis of the cells. Scale bar, 5 μm. Data presented are representative of three independent experiments. (C) Structure illumination microscopy analysis of the cells. Scale bar, 5 μm. Data presented are representative of three independent experiments. (D) Fifty randomly selected cells from panel B were analyzed for the infection stage at 1.5 h, 2.5 h, and 4 h. Based on GFP localization, the cells were classified into three categories of infection stages: early (punctate fluorescence or continuous fluorescence at the plasma membrane), intermediate (diffuse cytoplasmic fluorescence near the plasma membrane), and late (cytoplasmic granular fluorescence). (E) BHK-21 cells were transfected with a plasmid expressing mCherry or TMEM45B-mCherry. At 24 h posttransfection, the cells were incubated with SVNI-Nsp3-GFP at an MOI of 500 PFU/cell at 4°C for 1 h and then shifted to 37°C. At 6 h postinfection, the cells were stained with anti-dsRNA antibody and Alexa 680-conjugated secondary antibody and analyzed by confocal fluorescence microscopy. Scale bar, 10 μm. Data presented are representative of three independent experiments. (F) Fifty randomly selected cells at 6 h postinfection in panel E were analyzed for infection stage, as described above. EV, mCherry; 45B, TMEM45B-mCherry.

TMEM45B interacts with CHIKV Nsp1 and Nsp4. To probe whether TMEM45B may also inhibit the replication of other alphaviruses, we analyzed the interactions of TMEM45B with the nonstructural proteins of CHIKV. Coimmunoprecipitation assays revealed that TMEM45B interacted with CHIKV Nsp1 and Nsp4 (Fig. 8A). Confocal microscopy analysis showed that TMEM45B colocalized with Nsp1 and Nsp4 (Fig. 8B),

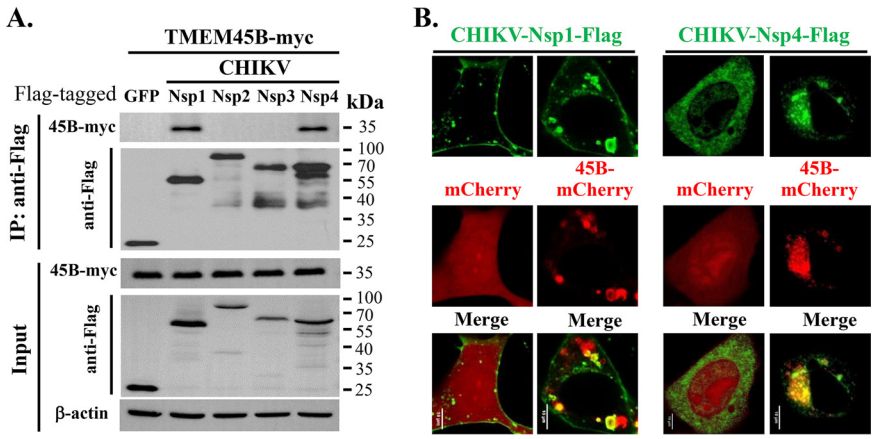

FIG 8 TMEM45B interacts with CHIKV Nsp1 and Nsp4. (A) Flag-tagged CHIKV Nsp1, Nsp2, Nsp3, Nsp4, or GFP was transiently coexpressed with TMEM45B-myc in 293T cells. At 48 h posttransfection, cell lysates were immunoprecipitated with Anti-Flag affinity gel, and the precipitated proteins were analyzed by Western blotting. (B) The proteins indicated were transiently coexpressed with mCherry or TMEM45B-mCherry in BHK-21 cells. At 16 h posttransfection, cells were fixed in paraformaldehyde, stained with anti-Flag antibody and Alexa 488-conjugated secondary antibody, and analyzed by confocal fluorescence microscopy. Scale bar, 10 μm. Data presented are representative of three independent experiments. 45B, TMEM45B.

further supporting the interactions of TMEM45B with CHIKV Nsp1 and Nsp4. These results suggest that TMEM45B might also inhibit the replication of CHIKV, though further investigation is needed to prove or disprove it.

DISCUSSION

IFN potently inhibits SINV replication, and multiple IFN-stimulated host antiviral factors have been reported to inhibit the viral replication through a variety of mechanisms. However, host antiviral factors targeting the viral nonstructural proteins have not been documented. Here, we showed that the IFN-stimulated gene product TMEM45B interacted with Nsp1 and Nsp4, interfered with the interaction between Nsp1 and Nsp4, and inhibited SINV replication.

The genome replication of plus-strand RNA viruses infecting eukaryotic cells is associated with cellular membranes. The membranes can be derived from the endoplasmic reticulum or other organelles of the secretory pathway or from the endolysosomal compartments. The membrane association provides a structural framework for replication, fixes the RNA replication process to a spatially confined place, increasing the local concentration of necessary components, and offers protection for the alien RNA molecules from the host defense mechanisms (65–69). Following the release of viral genomic RNA of infecting SINV from the early endosome, the viral protein synthesis is believed to take place on the rough ER. The newly synthesized viral proteins in complex with the viral genomic RNA associate with the intracellular membrane and migrate to the plasma membrane. TMEM45B is localized on the *trans*-Golgi network, late endosomes, and lysosomes (Fig. 2A), the organelles the viral complex would encounter during the migration. It is conceivable that the interaction of TMEM45B with the key components of the viral replication complex, Nsp1 and Nsp4 (Fig. 3), could interfere with the association of the viral complex with the intracellular membrane. Furthermore, Nsp1 plays a critical role in the capping of newly synthesized viral RNA, and the interaction of TMEM45B with Nsp1 may interfere with this process. These reasonings would explain how TMEM45B reduced the protein levels expressed from the viral RNA (Fig. 4), destabilized the viral RNA (Fig. 5), and rendered the viral RNA sensitive to RNase treatment (Fig. 6). Nonetheless, further investigation is needed to better understand the mechanisms for the inhibition of viral protein expression by TMEM45B.

We noticed that the expression of TMEM45B did not significantly affect the viral

protein levels on the plasma membrane (Fig. 7), which appears to be inconsistent with the above results. A plausible explanation is that in the experiments described above, the cells were infected with SINV at an MOI of 20 PFU/cell. However, to detect the GFP signals, the cells were infected with the virus at an MOI of 500 PFU/cell. Under this condition, the inhibitory effect of TMEM45B on the viral protein level and RNA stability could be overwhelmed. In addition, TMEM45B was not localized on the plasma membrane and thus should not affect the formation of spherules on the plasma membrane.

The detailed process of SINV-induced CPV formation is not yet very clear. With the amplification of the viral replication complex, the spherules grow and migrate toward the nucleus. In this process, the spherules need to capture more membranes to form CPVs. The results that TMEM45B is localized on endosomes and lysosomes and that the virus-induced CPVs were barely detectable in TMEM45B-expressing cells suggest that the growing spherules likely capture the membranes along with TMEM45B from these organelles, which inhibits the viral replication and thus prevents formation of the virus-induced CPVs.

Based on the results presented in this report and the above discussion, we propose a working model for TMEM45B. TMEM45B interacts with Nsp1 and Nsp4 and thus interferes with the association of the viral complex on the intracellular membrane, where TMEM45B resides. This leads to the reduction in the protein levels expressed from the viral RNA to some extent. The viral replication complex that escapes TMEM45B migrates to the plasma membrane to form spherules, where TMEM45 is absent. When the spherules grow and migrate toward the nucleus, TMEM45B on the membrane of endosomes or/and lysosomes is brought to the vicinity of the replication complex. TMEM45B interferes with the interaction between Nsp1 and Nsp4, inhibits the viral genome replication, and thus prevents the formation of the virus-induced CPVs.

In summary, here we identified TMEM45B as an antiviral factor against SINV. Analyses of the mechanisms by which TMEM45B inhibits the viral replication help to better understand the detailed process of the viral genome replication.

MATERIALS AND METHODS

Plasmids. The coding sequences of TMEM45B, XAF1, and HuR were PCR amplified from 293T cell cDNA and cloned into the expression vector pLPCX-3myc (Clontech) with a triple myc tag at the C terminus. pLPCX-NZAP-Zeo-3myc, which expresses the N-terminal 254 amino acids of rat ZAP fused to the Zeocin resistance gene, has been described previously (70). pcDNA4-mCherry and pcDNA4-TMEM45B-mCherry, which express mCherry and TMEM45B fused with mCherry at the C terminus, respectively, were generated by cloning the coding sequences into the mammalian expression vector pcDNA4 (Invitrogen). pSVNI and pToto1101 are infectious clones of SINV and have been reported previously (54, 71, 72). Plasmids pSVNI-Nsp3-nLuc, pToto1101-Nsp3-Luc-Pol$^-$ (herein pSINV-Nsp3-Luc-Pol$^-$), and pToto1101-Nsp3-Luc-ts6 (herein pSINV-Nsp3-Luc-ts6) were generous gifts from Margaret MacDonald of The Rockefeller University. The plasmid pSVNI-Nsp3-GFP was constructed by in-frame insertion of the GFP coding sequence into the SpeI site in the Nsp3-coding region of pSVNI. SVNI-Flag-Nsp1 was constructed by insertion of a tandem Flag tag at the N terminus of Nsp1 in SVNI. The plasmids pSINV-Nsp3-nLuc-Pol$^-$ and pSINV-Nsp3-nLuc-ts6 were generated by replacing the coding sequence of firefly luciferase with that of the nanoluciferase in pSINV-Nsp3-Luc-Pol$^-$ and pSINV-Nsp3-Luc-ts6, respectively. The coding sequences of SINV Nsp1, Nsp2, Nsp3, and Nsp4 from pSVNI were cloned into the protein expression vector pcDNA4 with a Flag tag at the C terminus. The coding sequences of CHIKV Nsp1, Nsp2, Nsp3, and Nsp4, generous gifts from Zhang Bo of the Wuhan Institute of Virology, were cloned into pcDNA4 with a Flag tag at the C terminus. To express Nsp1-EGFP and Nsp4-EGFP, the coding sequences of Nsp1 and Nsp4 were cloned into pEGFP-N1 (Clontech) to generate pEGFP-N1-Nsp1 and pEGFP-N1-Nsp4. To generate the construct expressing TMEM45B-ECFP, the coding sequence of TMEM45B was cloned into pECFP-N1 (Clontech). Plasmids expressing organelle markers pDsRed2-ER, pTGN38-mCherry, pLamp1-mCherry, pDsRed2-Rab5, and pRab7-RFP were generous gifts from Li Yu of Tsinghua University. All plasmid constructions were verified by DNA sequencing.

Cell culture. Cells were grown in Dulbecco's modified Eagle's medium (DMEM) (Invitrogen) supplemented with 10% fetal bovine serum (FBS) (Gibco). Plasmid transfection was performed using Xpregen following the manufacturer's instructions (Beijing Yu-Feng Biotechnology). To downregulate endogenous TMEM45B expression, 293A cells were seeded in 35-mm tissue culture dishes. The cells were transfected with 150 pmol of a control siRNA or an siRNA targeting TMEM45B using Lipofectamine 2000 (Invitrogen). The target sequences of the siRNAs (GenePharma) are as follows: control siRNA, 5′-UUCUCCGAACGUGUCACGUTT-3′; siTMEM45B-1, 5′-CACUGGAUAAAGUUAAUGATT-3′; siTMEM45B-2, 5′-GCCGCAAUUAGGACUUUGUTT-3′.

Virus production, titration, and infection. The reporter viruses SVNI-Nsp3-nLuc, SVNI-Nsp3-GFP, SVNI-Flag-Nsp1, and SINV-Nsp3-nLuc-ts6 were produced and titrated essentially as previously reported (44). Briefly, the infectious clones were linearized with XhoI and *in vitro* transcribed into RNA with SP6

RNA polymerase (Promega) in the presence of a cap analog (Promega). The 5′-capped transcripts were transfected into BHK-21 cells using Lipofectamine 2000 (Invitrogen) by following the manufacturer's instructions. At 24 h posttransfection, the virus in the culture supernatant was harvested and stored at −80°C. Virus stocks and virus samples were titrated in duplicate by infection of BHK-21 cells at serial dilutions in DMEM supplemented with 1% FBS. At 1 h postinfection, cells were covered with a DMEM overlay containing 1.2% agarose and 2% FBS. Plaques were enumerated at 1 to 2 days postinfection. For the temperature-sensitive SINV-Nsp3-nLuc-ts6, the virus was produced at the permissive temperature (28°C), and infection was carried out at 28°C or 40°C. The production and titration of influenza A virus IAV-Gluc have been previously described (73). Control cells or TMEM45B-expressing cells were infected with IAV-Gluc at an MOI of 0.01 PFU/cell at 37°C for 1 h. The cells were washed twice with phosphate-buffered saline (PBS) and cultured in DMEM supplemented with 2% fetal bovine serum. At 24 h postinfection, the cells were lysed and the *Gaussia* luciferase activity was measured.

Luciferase assay. For firefly luciferase, *Gaussia* luciferase, and nanoluciferase assays, cells were lysed in 5× luciferase cell culture lysis reagent (Promega). Luciferase activity was measured using the luciferase assay system (Promega) and the Nano-Glo luciferase assay system (Promega) by following the manufacturer's instructions.

Confocal microscopy. To monitor how TMEM45B inhibits SINV replication, pcDNA4-mCherry or pcDNA4-TMEM45B-mCherry was transfected into BHK-21 cells. At 24 h posttransfection, the cells were incubated with SVNI-Nsp3-GFP at an MOI of 500 PFU/cell for 1 h at 4°C and then shifted to 37°C. At various time points (1.5 h, 2.5 h, and 4 h postinfection), cells were fixed for 1 h with 4% paraformaldehyde, washed with PBS, and permeabilized with 0.2% Triton X-100. The cells were then stained with DAPI (4′,6-diamidino-2-phenylindole) (Beyotime Biotechnology; catalogue no. C-1005), washed 3 times with PBS, and photographed using a laser confocal microscope (Zeiss LSM700) or a structure illumination ultra-high-resolution fluorescence microscope (Applied Precision DeltaVision OMX-V3). To analyze the localization of the viral dsRNA, the cells were stained with anti-dsRNA antibody and Alexa 680-conjugated secondary antibody at 6 h postinfection. To analyze the localization of TMEM45B, the plasmid expressing TMEM45B-myc was transfected into BHK-21 or 293T cells together with a plasmid expressing a red fluorescent protein-tagged organelle marker. At 16 h posttransfection, the cells were fixed for 1 h with 4% paraformaldehyde, washed with PBS three times, and permeabilized with 0.2% Triton X-100. TMEM45B-myc was stained with anti-myc antibody and Alexa 488-conjugated secondary antibody and photographed using a laser confocal microscope (Zeiss LSM700). Microscopic analyses of the colocalization of TMEM45B with Nsp1 and Nsp4 were performed by similar procedures.

Virus binding assay. 293A cells were seeded at 10^6 cells/35-mm tissue culture dish. The next day, the cells were transfected with 150 pmol of a control siRNA or an siRNA targeting TMEM45B using Lipofectamine 2000 (Invitrogen). At 48 h posttransfection, the cells were incubated with 2×10^7 PFU of SVNI-Nsp3-nLuc in binding medium (DMEM supplemented with 1% FBS). Binding was carried out on a rocker at 4°C for 1 h with frequent additional manual rocking. The cells were then washed five times with 2 mL of PBS at 4°C per well. The total RNA was extracted using TRIzol reagent (Invitrogen), followed by reverse transcription with murine leukemia virus (MLV) reverse transcriptase using random primers. The levels of SINV genomic RNA were measured by SYBR green real-time PCR in a Rotor Gene 6000 (Corbett Life Science), using GAPDH (glyceraldehyde-3-phosphate dehydrogenase) mRNA as an internal control.

Membrane flotation assay. Cell fractionation and sucrose gradient centrifugation assays were modified from those reported previously (74). Briefly, 5×10^6 293T cells were infected with SVNI-Nsp3-nLuc at an MOI of 20 PFU/cell for 1.5 h at 37°C. The cells were trypsinized, washed with PBS twice, and resuspended in 0.5 mL TE buffer (10 mM Tris-HCl [pH 7.5], 4 mM EDTA) supplemented with the cOmplete protease inhibitor cocktail (Roche). The samples were prepared using a Dounce homogenizer to remove nuclei and residual cells as described previously (75). After low-speed centrifugation (510 × *g*, 10 min, 4°C), the postnuclear supernatant (PNS) was adjusted to 150 mM NaCl and mixed with 85% (wt/vol) sucrose in TNE buffer (25 mM Tris-HCl [pH 7.5], 150 mM NaCl, 4 mM EDTA) and loaded at the bottom of a centrifuge tube. On top of this PNS-containing 73% (wt/vol) sucrose mixture was layered 65% and 10% (wt/vol) sucrose in TNE. The gradients were centrifuged in a P40ST rotor at 100,000 × *g* for 18 h at 4°C (Himac CP100NX). Eleven fractions, 1 mL each, were collected, and 1 mL TNE buffer was added to the bottom of the tube to collect the remaining sample. Each fraction was equally divided into three aliquots. One aliquot was used for Western analysis. The other two were used for the analysis of RNA levels: one was untreated and one was treated with RNase A for 30 min. At the end of the treatment, TRIzol (Invitrogen) was added to the samples, followed by the addition of *in vitro*-transcribed IAV NS1 RNA to serve as a sample handling control. The RNA was extracted and analyzed by RT-qPCR using the NS1 RNA as a control.

Cell fractionation assay. The cell fractionation experimental procedure was adapted from published papers (60, 76, 77). 293T cells in four confluent 10-cm dishes were washed with ice-cold PBS, trypsinized, washed with PBS twice, and resuspended in 1 mL of ice-cold sucrose homogenization buffer (0.25 mM sucrose, 1 mM EDTA, pH 7.4) supplemented with the cOmplete protease inhibitor cocktail (Roche). The cells were homogenized using a Dounce homogenizer with 40 strokes and centrifuged for 10 min at 1,000 × *g* at 4°C to pellet nuclei and residual cells. The postnuclear supernatant (PNS) was loaded on iodixanol gradients (0.5%, 1%, 2.5%, 5%, 7.5%, 10%, 12.5%, 15%, 17.5%, 20%, 25%, and 30% [vol/vol] in 0.25 mM sucrose) and ultracentrifuged in a P40ST rotor at 100,000 × *g* for 1 h at 4°C (Himac CP100NX). Twenty-seven fractions, 444 μL each, were collected and analyzed by Western blotting.

RNA decay assay. Multiple dishes of 293A cells were transfected with an siRNA, and 293T cells were transfected with the empty vector pLPCX, pLPCX-TMEM45B-3myc, or pLPCX-HuR-myc. At 48 h posttransfection, the cells were incubated with SINV-Nsp3-nLuc-ts6 at an MOI of 20 PFU/cell for 1 h at 4°C. Some

dishes of the cells were shifted to 28°C for 24 h, followed by analysis for luciferase activity and protein expression, and the other dishes of the cells were transferred to the nonpermissive temperature (40°C) to shut off viral transcription. At various time points after shutoff, total RNA was extracted with TRIzol (Invitrogen). The viral RNA levels were measured by RT-qPCR with the SINV genomic RNA primers (Nsp4-F and Nsp4-R), using GAPDH mRNA as an internal control.

Coimmunoprecipitation assay. To analyze the interaction of TMEM45B with the nonstructural proteins, 293T cells were transfected with a plasmid expressing Flag-tagged GFP, Nsp1, Nsp2, Nsp3, or Nsp4 and a plasmid expressing myc-tagged TMEM45B. At 48 h posttransfection, cells were lysed in cell culture lysis reagent (Sigma-Aldrich), and the clarified cell lysates were mixed with the anti-Flag M2 affinity gel (Sigma-Aldrich) at 4°C for 4 h. The resins were washed with TBST (20 mM Tris-HCl [pH 7.6], 150 mM NaCl, 0.1% Tween 20) five times, and bound proteins were analyzed by Western blotting. To analyze whether TMEM45B interferes with the interaction between Nsp1 and Nsp4, 293T cells were cotransfected with a plasmid expressing Flag-tagged Nsp4 or GFP and a plasmid expressing myc-tagged Nsp1 or TMEM45B. At 48 h posttransfection, the cell lysates were immunoprecipitated with Anti-Flag affinity gel and the associated proteins were analyzed by Western blotting.

Antibodies. All the antibodies were commercially purchased, including the mouse monoclonal antibody against β-actin (GSGB-Bio, China; catalogue no. TA-09), myc-specific mouse monoclonal antibody 9E10 (Santa Cruz Biotechnology; catalogue no. SC-40), Flag-specific mouse monoclonal antibody M2 (Sigma-Aldrich; catalogue no. F3165-5MG), goat TMEM45B-specific antibody (Santa Cruz Biotechnology; catalogue no. SC-244436), rabbit Lamp1 polyclonal antibody (Proteintech; catalogue no. 21997-1-AP), rabbit calnexin polyclonal antibody (Proteintech; catalogue no. 10427-2-AP), mouse anti-dsRNA J2 monoclonal antibody (Scicons; catalogue no. 10010200), goat anti-mouse IgG (H+L)–horseradish peroxidase (HRP) conjugate (Promega; catalogue no. W4021), goat anti-rabbit IgG (H+L)–peroxidase conjugate (ZSGB-Bio; catalogue no. ZB2301), goat polyclonal secondary antibody to mouse IgG(H+L)-Alexa Fluor 488 conjugate (Abcam; catalogue no. ab150113), and donkey anti-mouse IgG (H+L) highly cross-adsorbed secondary antibody Alexa Fluor Plus 680 IgG (Invitrogen; catalogue no. A32788).

RNA immunoprecipitation assay. To analyze the influence of TMEM45B on the interaction of the Nsp1 with the viral RNA, 293T cells were transfected with an empty vector or a plasmid expressing TMEM45B-myc. At 48 h posttransfection, the cells were infected with SVNI-Flag-Nsp1 at an MOI of 20 PFU/cell for 6 h at 37°C. The cells were lysed in cell culture lysis reagent (Sigma-Aldrich), and clarified cell lysates were mixed with Anti-Flag M2 affinity gel (Sigma-Aldrich) at 4°C for 4 h. The resins were washed with TBST (20 mM Tris-HCl [pH 7.6], 150 mM NaCl, 0.1% Tween 20) five times and equally divided into two aliquots. One aliquot was used for Western analysis, and the other was used to detect the negative-strand viral RNA. The RNA was extracted with TRIzol and reverse transcribed with a mixture of negative-strand viral RNA-specific primers, followed by qPCR quantification using primers Nsp4-F and Nsp4-R (see below). Sequences of the reverse transcription primers are as follows: RT-1, 5′-CCAGTAAACTAATCGAGCTG-3′; RT-2, 5′-CGGATATATCACCTGACGAT-3′; RT-3, 5′-ATGG CCCCGCCAAGAATACA-3′; RT-4, 5′-CATCCCACTAACGTACCATC-3′; RT-5, 5′-AGTCTGTCGCCATTCCACTG-3′; RT-6, 5′-CGGATCAATTTTCGACGGAG-3′; RT-7, 5′-CTCCAGTAGCGTACCGGCGA-3′; RT-8, 5′-GAGCAAGACGAAGA CAGAAG-3′; RT-9, 5′-CAATTAGATACAGACCACTT-3′; and RT-10, 5′-AGTCGACAGTACATGTCCTG-3′.

Real-time PCR. Total RNA was extracted using TRIzol reagent by following the manufacturer's instructions and reverse transcribed with MLV reverse transcriptase using random primers or specific primers. The RNA levels were measured by SYBR green real-time PCR in a Rotor Gene 6000 (Corbett Life Science) using the following program: (i) 50°C for 2 min, 1 cycle; (ii) 95°C for 5 min, 1 cycle; (iii) 95°C for 15 s, 60°C for 30 s, and 72°C for 30 s, 40 cycles; and (iv) 72°C for 10 min, 1 cycle. Sequences of the PCR primers are as follows: SINV Nsp4-F, 5′-CATCGGTGAGAGACCACCTT-3′; SINV Nsp4-R, 5′-AACCACGCCTT TGTTTCATC-3′; GAPDH-F, 5′-CAACAGCAACTCCCACTCTTC-3′; GAPDH-R, 5′-GGTCCAGGGTTTCTTACTCC TT-3′; IAV NS1-F, 5′-AGAACTAGGTGATGCCCCATTCCTTGATCG-3′; IAV NS1-R, 5′-GCCAACAATTGTCCCCT CTTCGGTGAAGGC-3′; Renilla-F, 5′- TGAGGCACTGGGCAGGTGTC-3′; and Renilla-R, 5′- ATGAAGGAGTCC AGCACGTTC-3′.

Statistical analysis. Excel software (Microsoft) and GraphPad Prism were used to determine average values and standard deviations (SD). Mean values ± SD were calculated from three independent experiments unless otherwise indicated, and *P* values were calculated using the two-tailed paired Student's *t* test. *P* values are indicated in the figures as follows: *, $P < 0.05$; **, $P < 0.01$; ***, $P < 0.001$; ****, $P < 0.0001$; n.s. (nonsignificant), $P > 0.05$.

ACKNOWLEDGMENTS

We are grateful to Margaret MacDonald of The Rockefeller University and Zhang Bo of Wuhan Institute of Virology for providing the plasmids.

This work was supported by grants to Guangxia Gao from the Ministry of Science and Technology of China (grant no. 2018YFA0507202), the Chinese Academy of Sciences (grant no. XDB29010206) and the National Natural Science Foundation of China (grant no. 81921005).

REFERENCES

1. Forrester NL, Palacios G, Tesh RB, Savji N, Guzman H, Sherman M, Weaver SC, Lipkin WI. 2012. Genome-scale phylogeny of the alphavirus genus suggests a marine origin. J Virol 86:2729–2738. https://doi.org/10.1128/JVI.05591-11.

2. Nasar F, Palacios G, Gorchakov RV, Guzman H, Da Rosa AP, Savji N, Popov VL, Sherman MB, Lipkin WI, Tesh RB, Weaver SC. 2012. Eilat virus, a unique alphavirus with host range restricted to insects by RNA replication. Proc Natl Acad Sci U S A 109:14622–14627. https://doi.org/10.1073/pnas.1204787109.
3. Jose J, Snyder JE, Kuhn RJ. 2009. A structural and functional perspective of alphavirus replication and assembly. Future Microbiol 4:837–856. https://doi.org/10.2217/fmb.09.59.
4. DeTulleo L, Kirchhausen T. 1998. The clathrin endocytic pathway in viral infection. EMBO J 17:4585–4593. https://doi.org/10.1093/emboj/17.16.4585.
5. Hammar L, Markarian S, Haag L, Lankinen H, Salmi A, Cheng RH. 2003. Prefusion rearrangements resulting in fusion peptide exposure in Semliki Forest virus. J Biol Chem 278:7189–7198. https://doi.org/10.1074/jbc.M206015200.
6. Wahlberg JM, Bron R, Wilschut J, Garoff H. 1992. Membrane fusion of Semliki Forest virus involves homotrimers of the fusion protein. J Virol 66:7309–7318. https://doi.org/10.1128/JVI.66.12.7309-7318.1992.
7. Wahlberg JM, Garoff H. 1992. Membrane fusion process of Semliki Forest virus. I. Low pH-induced rearrangement in spike protein quaternary structure precedes virus penetration into cells. J Cell Biol 116:339–348. https://doi.org/10.1083/jcb.116.2.339.
8. Singh I, Helenius A. 1992. Role of ribosomes in Semliki Forest virus nucleocapsid uncoating. J Virol 66:7049–7058. https://doi.org/10.1128/JVI.66.12.7049-7058.1992.
9. Wengler G, Würkner D, Wengler G. 1992. Identification of a sequence element in the alphavirus core protein which mediates interaction of cores with ribosomes and the disassembly of cores. Virology 191:880–888. https://doi.org/10.1016/0042-6822(92)90263-O.
10. Laakkonen P, Ahola T, Kaariainen L. 1996. The effects of palmitoylation on membrane association of Semliki Forest virus RNA capping enzyme. J Biol Chem 271:28567–28571. https://doi.org/10.1074/jbc.271.45.28567.
11. Frolova E, Gorchakov I, Pereboeva R, Atasheva L, Frolov S. 2010. Functional Sindbis virus replicative complexes are formed at the plasma membrane. J Virol 84:11679–11695. https://doi.org/10.1128/JVI.01441-10.
12. Spuul P, Salonen A, Merits A, Jokitalo E, Kääriäinen L, Ahola T. 2007. Role of the amphipathic peptide of Semliki Forest virus replicase protein nsP1 in membrane association and virus replication. J Virol 81:872–883. https://doi.org/10.1128/JVI.01785-06.
13. Lemm JA, Rice CM. 1993. Roles of nonstructural polyproteins and cleavage products in regulating Sindbis virus RNA replication and transcription. J Virol 67:1916–1926. https://doi.org/10.1128/JVI.67.4.1916-1926.1993.
14. Mai J, Sawicki SG, Sawicki DL. 2009. Fate of minus-strand templates and replication complexes produced by a P23-cleavage-defective mutant of Sindbis virus. J Virol 83:8553–8564. https://doi.org/10.1128/JVI.00056-09.
15. Lemm JA, Rümenapf T, Strauss EG, Strauss JH, Rice CM. 1994. Polypeptide requirements for assembly of functional Sindbis virus replication complexes: a model for the temporal regulation of minus- and plus-strand RNA synthesis. EMBO J 13:2925–2934. https://doi.org/10.1002/j.1460-2075.1994.tb06587.x.
16. Shirako Y, Strauss JH. 1994. Regulation of Sindbis virus RNA replication: uncleaved P123 and nsP4 function in minus-strand RNA synthesis, whereas cleaved products from P123 are required for efficient plus-strand RNA synthesis. J Virol 68:1874–1885. https://doi.org/10.1128/JVI.68.3.1874-1885.1994.
17. Ahola T, Lampio A, Auvinen P, Kääriäinen L. 1999. Semliki Forest virus mRNA capping enzyme requires association with anionic membrane phospholipids for activity. EMBO J 18:3164–3172. https://doi.org/10.1093/emboj/18.11.3164.
18. Jones R, Bragagnolo G, Arranz R, Reguera J. 2021. Capping pores of alphavirus nsP1 gate membranous viral replication factories. Nature 589:615–619. https://doi.org/10.1038/s41586-020-3036-8.
19. Vasiljeva L, Merits A, Auvinen P, Kääriäinen L. 2000. Identification of a novel function of the alphavirus capping apparatus. RNA 5'-triphosphatase activity of Nsp2. J Biol Chem 275:17281–17287. https://doi.org/10.1074/jbc.M910340199.
20. Tomar S, Hardy RW, Smith JL, Kuhn RJ. 2006. Catalytic core of alphavirus nonstructural protein nsP4 possesses terminal adenylyltransferase activity. J Virol 80:9962–9969. https://doi.org/10.1128/JVI.01067-06.
21. Rubach JK, Wasik BR, Rupp JC, Kuhn RJ, Hardy RW, Smith JL. 2009. Characterization of purified Sindbis virus nsP4 RNA-dependent RNA polymerase activity in vitro. Virology 384:201–208. https://doi.org/10.1016/j.virol.2008.10.030.
22. Urakova N, Kuznetsova V, Crossman DK, Sokratian A, Guthrie DB, Kolykhalov AA, Lockwood MA, Natchus MG, Crowley MR, Painter GR. 2018. β-D-N(4)-hydroxycytidine is a potent anti-alphavirus compound that induces high level of mutations in viral genome. J Virol 92:e01965-17. https://doi.org/10.1128/JVI.01965-17.
23. Li GP, La Starza MW, Hardy WR, Strauss JH, Rice CM. 1990. Phosphorylation of Sindbis virus nsP3 in vivo and in vitro. Virology 179:416–427. https://doi.org/10.1016/0042-6822(90)90310-n.
24. Vihinen H, Saarinen J. 2000. Phosphorylation site analysis of Semliki Forest virus nonstructural protein 3. J Biol Chem 275:27775–27783. https://doi.org/10.1074/jbc.M002195200.
25. Abraham R, Hauer D, McPherson RL, Utt A, Kirby IT, Cohen MS, Merits A, Leung AKL, Griffin DE. 2018. ADP-ribosyl-binding and hydrolase activities of the alphavirus nsP3 macrodomain are critical for initiation of virus replication. Proc Natl Acad Sci U S A 115:E10457–E10466. https://doi.org/10.1073/pnas.1812130115.
26. Abraham R, McPherson RL, Dasovich M, Badiee M, Leung AKL, Griffin DE. 2020. Both ADP-ribosyl-binding and hydrolase activities of the alphavirus nsP3 macrodomain affect neurovirulence in mice. mBio 11:e03253-19. https://doi.org/10.1128/mBio.03253-19.
27. Froshauer S, Kartenbeck J, Helenius A. 1988. Alphavirus RNA replicase is located on the cytoplasmic surface of endosomes and lysosomes. J Cell Biol 107:2075–2086. https://doi.org/10.1083/jcb.107.6.2075.
28. Kujala P, Ikäheimonen A, Ehsani N, Vihinen H, Auvinen P, Kääriäinen L. 2001. Biogenesis of the Semliki Forest virus RNA replication complex. J Virol 75:3873–3884. https://doi.org/10.1128/JVI.75.8.3873-3884.2001.
29. Kallio K, Hellström K, Balistreri G, Spuul P, Jokitalo E, Ahola T. 2013. Template RNA length determines the size of replication complex spherules for Semliki Forest virus. J Virol 87:9125–9134. https://doi.org/10.1128/JVI.00660-13.
30. Spuul P, Balistreri G, Kaariainen L, Ahola T. 2010. Phosphatidylinositol 3-kinase-, actin-, and microtubule-dependent transport of Semliki Forest virus replication complexes from the plasma membrane to modified lysosomes. J Virol 84:7543–7557. https://doi.org/10.1128/JVI.00477-10.
31. Grimley PM, Berezesky IK, Friedman RM. 1968. Cytoplasmic structures associated with an arbovirus infection: loci of viral ribonucleic acid synthesis. J Virol 2:1326–1338. https://doi.org/10.1128/JVI.2.11.1326-1338.1968.
32. Garoff H, Wilschut J, Liljeström P, Wahlberg JM, Bron R, Suomalainen M, Smyth J, Salminen A, Barth BU, Zhao H. 1994. Assembly and entry mechanisms of Semliki Forest virus. Arch Virol Suppl 9:329–338.
33. Griffiths G, Quinn P, Warren G. 1983. Dissection of the Golgi complex. I. Monensin inhibits the transport of viral membrane proteins from medial to trans Golgi cisternae in baby hamster kidney cells infected with Semliki Forest virus. J Cell Biol 96:835–850. https://doi.org/10.1083/jcb.96.3.835.
34. Der SD, Zhou A, Williams BR, Silverman RH. 1998. Identification of genes differentially regulated by interferon α, β, or γ using oligonucleotide arrays. Proc Natl Acad Sci U S A 95:15623–15628. https://doi.org/10.1073/pnas.95.26.15623.
35. de Veer MJ, Holko M, Frevel M, Walker E, Der S, Paranjape JM, Silverman RH, Williams BRG. 2001. Functional classification of interferon-stimulated genes identified using microarrays. J Leukoc Biol 69:912–920.
36. Schoggins JW, Rice CM. 2011. Interferon-stimulated genes and their antiviral effector functions. Curr Opin Virol 1:519–525. https://doi.org/10.1016/j.coviro.2011.10.008.
37. Poddar S, Hyde JL, Gorman MJ, Farzan M, Diamond MS. 2016. The interferon-stimulated gene IFITM3 restricts infection and pathogenesis of arthritogenic and encephalitic alphaviruses. J Virol 90:8780–8794. https://doi.org/10.1128/JVI.00655-16.
38. Weston S, Czieso S, White IJ, Smith SE, Wash RS, Diaz-Soria C, Kellam P, Marsh M. 2016. Alphavirus Restriction by IFITM Proteins. Traffic 17:997–1013. https://doi.org/10.1111/tra.12416.
39. Bréhin AC, Casadémont I, Frenkiel MP, Julier C, Sakuntabhai A, Desprès P. 2009. The large form of human 2',5'-oligoadenylate synthetase (OAS3) exerts antiviral effect against Chikungunya virus. Virology 384:216–222. https://doi.org/10.1016/j.virol.2008.10.021.
40. Kristiansen H, Gad HH, Eskildsen-Larsen S, Despres P, Hartmann R. 2011. The oligoadenylate synthetase family: an ancient protein family with multiple antiviral activities. J Interferon Cytokine Res 31:41–47. https://doi.org/10.1089/jir.2010.0107.
41. Diamond MS, Farzan M. 2013. The broad-spectrum antiviral functions of IFIT and IFITM proteins. Nat Rev Immunol 13:46–57. https://doi.org/10.1038/nri3344.
42. Hyde JL, Gardner CL, Kimura T, White JP, Liu G, Trobaugh DW, Huang C, Tonelli M, Paessler S, Takeda K, Klimstra WB, Amarasinghe GK, Diamond MS. 2014. A viral RNA structural element alters host recognition of nonself RNA. Science 343:783–787. https://doi.org/10.1126/science.1248465.

43. Reynaud JM, Kim DY, Atasheva S, Rasalouskaya A, White JP, Diamond MS, Weaver SC, Frolova EI, Frolov I. 2015. IFIT1 differentially interferes with translation and replication of alphavirus genomes and promotes induction of type I interferon. PLoS Pathog 11:e1004863. https://doi.org/10.1371/journal.ppat.1004863.
44. Bick MJ, Carroll JW, Gao G, Goff SP, Rice CM, MacDonald MR. 2003. Expression of the zinc-finger antiviral protein inhibits alphavirus replication. J Virol 77:11555–11562. https://doi.org/10.1128/jvi.77.21.11555-11562.2003.
45. Atasheva S, Akhrymuk M, Frolova EI, Frolov I. 2012. New PARP gene with an anti-alphavirus function. J Virol 86:8147–8160. https://doi.org/10.1128/JVI.00733-12.
46. Atasheva S, Frolova EI, Frolov I. 2014. Interferon-stimulated poly(ADP-ribose) polymerases are potent inhibitors of cellular translation and virus replication. J Virol 88:2116–2130. https://doi.org/10.1128/JVI.03443-13.
47. Ooi YS, Dubé M, Kielian M. 2015. BST2/tetherin inhibition of alphavirus exit. Viruses 7:2147–2167. https://doi.org/10.3390/v7042147.
48. Landis H, Simon-Jödicke A, Klöti A, Di Paolo C, Schnorr JJ, Schneider-Schaulies S, Hefti HP, Pavlovic J. 1998. Human MxA protein confers resistance to Semliki Forest virus and inhibits the amplification of a Semliki Forest virus-based replicon in the absence of viral structural proteins. J Virol 72:1516–1522. https://doi.org/10.1128/JVI.72.2.1516-1522.1998.
49. Lenschow DJ, Giannakopoulos NV, Gunn LJ, Johnston C, O'Guin AK, Schmidt RE, Levine B, Virgin H. 2005. Identification of interferon-stimulated gene 15 as an antiviral molecule during Sindbis virus infection in vivo. J Virol 79:13974–13983. https://doi.org/10.1128/JVI.79.22.13974-13983.2005.
50. Lenschow DJ, Lai C, Frias-Staheli N, Giannakopoulos NV, Lutz A, Wolff T, Osiak A, Levine B, Schmidt RE, García-Sastre A, Leib DA, Pekosz A, Knobeloch KP, Horak I, Virgin H. 2007. IFN-stimulated gene 15 functions as a critical antiviral molecule against influenza, herpes, and Sindbis viruses. Proc Natl Acad Sci U S A 104:1371–1376. https://doi.org/10.1073/pnas.0607038104.
51. Werneke SW, Schilte C, Rohatgi A, Monte KJ, Michault A, Arenzana-Seisdedos F, Vanlandingham DL, Higgs S, Fontanet A, Albert ML, Lenschow DJ. 2011. ISG15 is critical in the control of Chikungunya virus infection independent of UbE1L mediated conjugation. PLoS Pathog 7:e1002322. https://doi.org/10.1371/journal.ppat.1002322.
52. Xu D, Holko M, Sadler AJ, Scott B, Higashiyama S, Berkofsky-Fessler W, McConnell MJ, Pandolfi PP, Licht JD, Williams BR. 2009. Promyelocytic leukemia zinc finger protein regulates interferon-mediated innate immunity. Immunity 30:802–816. https://doi.org/10.1016/j.immuni.2009.04.013.
53. Zhang X, Yang W, Wang X, Zhang X, Tian H, Deng H, Zhang L, Gao G. 2018. Identification of new type I interferon-stimulated genes and investigation of their involvement in IFN-β activation. Protein Cell 9:799–807. https://doi.org/10.1007/s13238-018-0511-1.
54. Lustig S, Halevy M, Ben-Nathan D, Akov Y. 1992. A novel variant of Sindbis virus is both neurovirulent and neuroinvasive in adult mice. Arch Virol 122:237–248. https://doi.org/10.1007/BF01317186.
55. Okada N, Yamamoto T, Watanabe M, Yoshimura Y, Obana E, Yamazaki N, Kawazoe K, Shinohara Y, Minakuchi K. 2011. Identification of TMEM45B as a protein clearly showing thermal aggregation in SDS-PAGE gels and dissection of its amino acid sequence responsible for this aggregation. Protein Expr Purif 77:118–123. https://doi.org/10.1016/j.pep.2011.01.011.
56. Li Y, Guo W, Liu S, Zhang B, Yu BB, Yang B, Kan SL, Feng SQ. 2017. Silencing transmembrane protein 45B (TNEM45B) inhibits proliferation, invasion, and tumorigenesis in osteosarcoma cells. Oncol Res 25:1021–1026. https://doi.org/10.3727/096504016X14821477992177.
57. Shen K, Yu W, Yu Y, Liu X, Cui X. 2018. Knockdown of TMEM45B inhibits cell proliferation and invasion in gastric cancer. Biomed Pharmacother 104:576–581. https://doi.org/10.1016/j.biopha.2018.05.016.
58. Luo F, Yang K, Wang YZ, Lin D. 2018. TMEM45B is a novel predictive biomarker for prostate cancer progression and metastasis. Neo 65:815–821. https://doi.org/10.4149/neo_2018_170822N551.
59. Tang Q, Wang X, Gao G. 2017. The short form of the zinc finger antiviral protein inhibits influenza A virus protein expression and is antagonized by the virus-encoded NS1. J Virol 91:e01909-16. https://doi.org/10.1128/JVI.01909-16.
60. Graham JM, Ford T, Rickwood D. 1990. Isolation of the major subcellular organelles from mouse liver using Nycodenz gradients without the use of an ultracentrifuge. Anal Biochem 187:318–323. https://doi.org/10.1016/0003-2697(90)90463-j.
61. Shirako Y, Strauss EG, Strauss JH. 2000. Suppressor mutations that allow Sindbis virus RNA polymerase to function with nonaromatic amino acids at the N-terminus: evidence for interaction between nsP1 and nsP4 in minus-strand RNA synthesis. Virology 276:148–160. https://doi.org/10.1006/viro.2000.0544.
62. Hahn YS, Grakoui A, Rice CM, Strauss EG, Strauss JH. 1989. Mapping of RNA$^-$ temperature-sensitive mutants of Sindbis virus: complementation group F mutants have lesions in nsP4. J Virol 63:1194–1202. https://doi.org/10.1128/JVI.63.3.1194-1202.1989.
63. Sokoloski KJ, Dickson AM, Chaskey EL, Garneau NL, Wilusz CJ, Wilusz J. 2010. Sindbis virus usurps the cellular HuR protein to stabilize its transcripts and promote productive infections in mammalian and mosquito cells. Cell Host Microbe 8:196–207. https://doi.org/10.1016/j.chom.2010.07.003.
64. Ahola T, Kääriäinen L. 1995. Reaction in alphavirus mRNA capping: formation of a covalent complex of nonstructural protein nsP1 with 7-methyl-GMP. Proc Natl Acad Sci U S A 92:507–511. https://doi.org/10.1073/pnas.92.2.507.
65. Sreevalsan T. 1970. Association of viral ribonucleic acid with cellular membranes in chick embryo cells infected with Sindbis virus. J Virol 6:438–444. https://doi.org/10.1128/JVI.6.4.438-444.1970.
66. Lorizate M, Kräusslich HG. 2011. Role of lipids in virus replication. Cold Spring Harb Perspect Biol 3:a004820. https://doi.org/10.1101/cshperspect.a004820.
67. Miller S, Krijnse-Locker J. 2008. Modification of intracellular membrane structures for virus replication. Nat Rev Microbiol 6:363–374. https://doi.org/10.1038/nrmicro1890.
68. Neufeldt CJ, Joyce MA, Van Buuren N, Levin A, Kirkegaard K, Gale M, Jr, Tyrrell DL, Wozniak RW. 2016. The hepatitis C virus-induced membranous web and associated nuclear transport machinery limit access of pattern recognition receptors to viral replication sites. PLoS Pathog 12:e1005428. https://doi.org/10.1371/journal.ppat.1005428.
69. Salonen A, Ahola T, Kääriäinen L. 2005. Viral RNA replication in association with cellular membranes. Curr Top Microbiol Immunol 285:139–173. https://doi.org/10.1007/3-540-26764-6_5.
70. Gao G, Guo X, Goff SP. 2002. Inhibition of retroviral RNA production by ZAP, a CCCH-type zinc finger protein. Science 297:1703–1706. https://doi.org/10.1126/science.1074276.
71. Scheidel LM, Stollar V. 1991. Mutations that confer resistance to mycophenolic acid and ribavirin on Sindbis virus map to the nonstructural protein nsP1. Virology 181:490–499. https://doi.org/10.1016/0042-6822(91)90881-B.
72. Rosenblum CI, Scheidel LM, Stollar V. 1994. Mutations in the nsP1 coding sequence of Sindbis virus which restrict viral replication in secondary cultures of chick embryo fibroblasts prepared from aged primary cultures. Virology 198:100–108. https://doi.org/10.1006/viro.1994.1012.
73. Pan W, Dong Z, Li F, Meng W, Feng L, Niu X, Li C, Luo Q, Li Z, Sun C, Chen L. 2013. Visualizing influenza virus infection in living mice. Nat Commun 4:2369. https://doi.org/10.1038/ncomms3369.
74. Pietilä MK, van Hemert MJ, Ahola T. 2018. Purification of highly active alphavirus replication complexes demonstrates altered fractionation of multiple cellular membranes. J Virol 92:e01852-17. https://doi.org/10.1128/JVI.01852-17.
75. Pietilä MK, Albulescu IC, Hemert MJV, Ahola T. 2017. Polyprotein processing as a determinant for in vitro activity of Semliki Forest virus replicase. Viruses 9:292. https://doi.org/10.3390/v9100292.
76. Ghosh S, Dellibovi-Ragheb TA, Kerviel A, Pak E, Qiu Q, Fisher M, Takvorian PM, Bleck C, Hsu VW, Fehr AR, Perlman S, Achar SR, Straus MR, Whittaker GR, de Haan CAM, Kehrl J, Altan-Bonnet G, Altan-Bonnet N. 2020. β-Coronaviruses use lysosomes for egress instead of the biosynthetic secretory pathway. Cell 183:1520–1535.e14. https://doi.org/10.1016/j.cell.2020.10.039.
77. Majer O, Liu B, Kreuk LSM, Krogan N, Barton GM. 2019. UNC93B1 recruits syntenin-1 to dampen TLR7 signalling and prevent autoimmunity. Nature 575:366–370. https://doi.org/10.1038/s41586-019-1612-6.